Available online at www.sciencedirect.com
ScienceDirect
Lithos xx (2007) xxx–xxx
LITHOS
www.elsevier.com/locate/lithos

Petrology and geochemistry of Zijinshan alkaline intrusive complex in Shanxi Province, western North China Craton: Implication for magma mixing of different sources in an extensional regime

Jifeng Ying [a,*], Hongfu Zhang [a], Min Sun [b], Yanjie Tang [a], Xinhua Zhou [a], Xiaoming Liu [c]

[a] *State Key Laboratory of Lithospheric Evolution, Institute of Geology and Geophysics, Chinese Academy of Sciences, P.O. Box 9825, Beijing 100029, China*
[b] *Department of Earth Sciences, The University of Hong Kong, Porkfulam road, Hong Kong, China*
[c] *Department of Geology, Northwest University, Xi'an 710069, China*

Received 14 June 2006; accepted 13 February 2007

Abstract

In situ zircon U–Pb ages and Hf isotopic compositions and whole rock geochemical and Sr–Nd–Pb isotopic data are presented for the Zijinshan alkaline intrusive complex from the Shanxi Province, western North China Craton. Salic rocks dominate the complex with the monzonite occurring in the outermost and pseudoleucite phonolitic breccia in the center. The intrusion took place 127 Ma ago with the earliest emplacement of monzonite and the termination of cryptoexplosive pseudoleucite phonolitic breccia. All rocks from this complex show LREE enrichment and HFSE depletion and exhibit enriched to depleted Sr–Nd isotopic features. The presence of inherited zircons and enriched Hf isotopic compositions in zircon rims, along with the enriched whole rock Sr–Nd isotopic compositions, indicate that the monzonite was formed through the mixing of lithospheric mantle-derived magma with lower crust-derived melts. The diopside syenite and nepheline-bearing diopside syenite are more depleted than the monzonite in terms of the Sr and Nd isotopes, together with their very high concentrations of LILE, we proposed that they originated from a mixed mantle source of enriched lithospheric mantle and depleted asthenosphere. The nepheline syenite has very low concentrations of MgO, Ni, Cr, suggesting that the magma underwent significant crystal fractionation. The most depleted Sr and Nd isotopic compositions ($(^{87}Sr/^{86}Sr)_i$=0.7036–0.7042, $\varepsilon_{Nd}(t)$=−0.2–0.3) among all rock types indicate a great contribution of asthenosphere to the nepheline syenite. The Zijinshan complex and its related crust-mantle interaction occurred in an extensional environment which resulted in continuously asthenospheric upwelling. Such an extensional environment might have been developed during the post-orogenic stage of the Late Paleozoic amalgamation of North China Craton with Mongolian continents and subsequent Mongol–Okhotsk ocean closure.
© 2007 Elsevier B.V. All rights reserved.

Keywords: Alkaline complex; Crust–mantle interaction; Monzonite; Nepheline syenite; North China Craton

1. Introduction

The evolution of the lithospheric mantle beneath the North China Craton (NCC) has attracted considerable attention over the past decades. Comparative studies on

* Corresponding author. Tel.: +86 10 62007821; fax: +86 10 62010846.
E-mail address: jfying@mail.igcas.ac.cn (J. Ying).

0024-4937/$ - see front matter © 2007 Elsevier B.V. All rights reserved.
doi:10.1016/j.lithos.2007.02.001

the Paleozoic kimberlite-borne mantle xenoliths and Cenozoic basalt-borne mantle xenoliths have revealed that the old, thick and refractory lithospheric mantle beneath the NCC was replaced by the young, thin and fertile mantle in the Mesozoic (Griffin et al., 1992; Menzies et al., 1993; Fan et al., 2000; Xu, 2001). Coincident with this catastrophic change in lithosphere is the widespread voluminous magmatism, the geochronological and geochemical investigation of the Mesozoic magmatism and relevant mantle xenoliths have provided valuable information on the timing and mechanism of such a considerable lithospheric change (Fan et al., 2001; Zhang et al., 2002; Zhang and Sun, 2002; Gao et al., 2004; Guo et al., 2004; Ying et al., 2004; Zhang, 2005; Ying et al., 2006). However, most of the above studies were confined to the east part of the NCC (to the east of DTGL, see next section). Compared to the tectonothermal reactivation of the eastern part of the NCC during the Mesozoic, the western part remains relatively stable since the Precambrian with only few magmatic activities in the Mesozoic. Thus, the nature and evolution of the mantle beneath the western part of NCC was less well-constrained due to the lack of magmatism.

In this paper, we report the geochronological, petrological and geochemical data of a Mesozoic alkaline intrusive complex–Zijinshan complex in the Linxian County, Shanxi Province, which tectonically locates in the western part of the NCC, with aims to constrain its petrogenesis and the tectonic evolution of the lithosphere beneath the western part of NCC.

2. Geologic background

The North China Craton (NCC), with Archean nucleus of 2.5–3.8 Ga, is the largest and oldest craton in China (Jahn et al., 1987; Liu et al., 1992). Geological and geophysical observations have revealed the existence of two large-scale N–S trending linear zones traversing the NCC, one is the Tan-Lu Fault in the east, and the other is the Daxing'anling–Taihang Gravity lineament (DTGL) in the west (Ma, 1989). The DTGL geophysical anomaly was traditionally regarded as the boundary between the eastern and western NCC, and this geophysical anomaly also coincides with the topographical anomaly from the east to west in the NCC. The eastern part mainly includes North China Plain, Shandong and Liaodong peninsula, and has a relatively thin crust (32–34 km) and lithosphere (60–80 km), while the western part include the Taihang Mountains, Lüliang Mountains and the Loess Plateau and has a relatively thick crust (greater than 40 km) and lithosphere (100 km) (Ma, 1989). Recently, a new tectonic division of the NCC was proposed according to the lithological, geochemical, and metamorphic P–T–t paths studies of the basement rocks, i.e. the NCC can be divided into three parts, the Eastern and Western Blocks and the Central Zone (Zhao et al., 2001). The Eastern Block is composed of early to late Archean orthogneisses intruded by 2.5 Ga syntectonic granitoids. The Western Block consists of late Archean to Paleoproterozoic metasedimentary belts which unconformably overlie Archean basement. The Central Zone, separating the Eastern and Western Block, is composed of late Archean amphibolites, granulites and 2.5 Ga greenstones which were overlain by bimodal volcanics and terrigenous sedimentary rocks. It was generally considered that the Eastern and Western Blocks evolved independently from the late Archean to early Paleoproterozoic before collided into a coherent craton along the Central Zone in Paleoproterozoic (1.85 Ga) (Zhao et al., 2001).

The Shanxi Province, situated at the central part of China, is bounded with two NE–SW trending mountain ranges, namely the Taihang Mountains in the east and the Lüliang Mountains in the west. Between the two mountain ranges occurs the Cenozoic Shanxi Graben system (Fig. 1).

Several alkaline intrusive complexes (Fig. 1b) have been found in Shanxi Province for a long history, but the studies for these complexes are scare and the available data are mainly petrological descriptions and some bulk rock compositions analyzed several decades ago.

As one of the earliest discovered alkaline intrusions, the Zijinshan complex locates about 20 km northeast of the Linxian County. Tectonically, this complex occurs in the boundary between the Western Block and the Central Zone of the NCC. This complex, intruding the Triassic Ermaying Group (sandstone and shale) exhibits a horseshoe shape with surface coverage of about 20 km^2. The main rock types, from the margin to the center, are monzonite, diopside syenite, nepheline-bearing diopside syenite, nepheline syenite, trachytic breccia, and pseudoleucite phonolitic breccia (Fig. 1c). Late stage dykes of varied compositions such as lamprophyres, carbonatites are frequently observed.

3. Petrography

3.1. Monzonite

Monzonite predominates in the outermost part of the complex and has the largest surface coverage. The intrusion of monzonite branches into the country rock sandstone can be sporadically seen. The rock is light-grey, medium-to coarse-grained with granular and

Please cite this article as: Ying, J. et al. Petrology and geochemistry of Zijinshan alkaline intrusive complex in Shanxi Province, western North China Craton: Implication for magma mixing of different sources in an extensional regime. Lithos (2007), doi:10.1016/j.lithos.2007.02.001

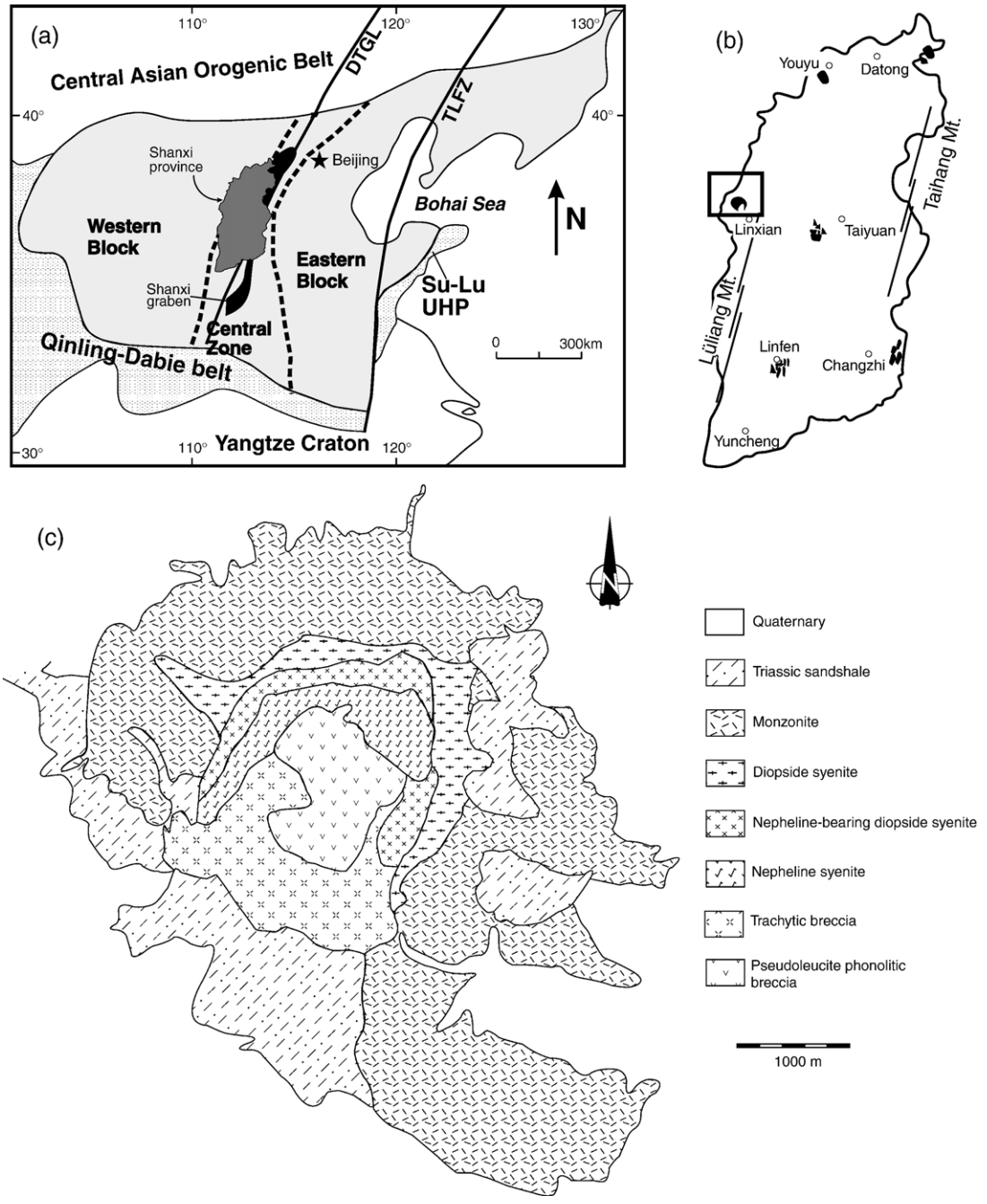


Fig. 1. (a) Simplified geological map showing the major tectonic units in eastern China and the location of Shanxi Province (Zhao et al., 2001). Also shown are two major geological and geophysical linear zones, the Daxing'anling–Taihang Gravity Lineament (DTGL) and the Tanlu Fault Zone (TLFZ) (Ma, 1989). (b) The outline of Shanxi Province and the distribution of alkaline intrusive rocks, the box shows the position of Zijinshan alkaline complex. (c) Geological sketch of the Zijinshan alkaline complex, modified after Wu et al. (1966) and Huang (1991).

porphyritic textures. It consists mainly of subhedral orthoclase lathes (45%), euhedral andesine lathes (40%), and diopside (10%) with subordinate amphibole, biotite and accessory zircon, titanite, apatite and magnetite.

3.2. Diopside syenite

Diopside syenite was previously named as aegirine–augite syenite merely according to the optical property

Please cite this article as: Ying, J. et al. Petrology and geochemistry of Zijinshan alkaline intrusive complex in Shanxi Province, western North China Craton: Implication for magma mixing of different sources in an extensional regime. Lithos (2007), doi:10.1016/j.lithos.2007.02.001

of the pyroxene. However, electron microprobe analyses in this study demonstrated that the pyroxene in this type of rock is diopside rather than aegirine–augite, and thus the rock should be named as diopside syenite. The rock is darkish-grey in color, medium-grained and subhedral granular texture. It shows massive and flow structure. The flow structure is defined by the oriented distribution of the diopside and amphibole. The rock is composed of orthoclase (50–70%), diopside (20–25%), amphibole (<5%) and biotite (5%). Accessory phases include titanite, apatite, magnetite, sodalite and melanite. The intrusion of diopside syenite into the monzonite and sporadically occurred monzonite enclaves in the diopside syenite suggests that the diopside syenite emplaced later than the monzonite.

3.3. Nepheline-bearing diopside syenite

Nepheline-bearing diopside syenite looks similar to diopside syenite except having a lower color index than that of diopside syenite. It has medium-grained, subhedral equigranular texture, massive and occasional flow structure. The rock-forming minerals include the dominant orthoclase (50–70%), diopside (15–20%) and nepheline (5%) and subordinate biotite, melanite, titanite, apatite and magnetite.

3.4. Nepheline syenite

Nepheline syenite is darkish-grey, coarse-grained massive rock and shows great variation in texture and mineral contents. Pegmatitic texture can also be seen within the body. The rock consists mainly of orthoclase, nepheline, diopside, melanite and biotite with accessory apatite and titanite. The orthoclase could be replaced by nepheline and the nepheline was then partially replaced by feldspathoid mineral such as sodalite. The occurrence of aggregates which consist of mafic minerals such as diopside, melanite and biotite is a typical feature of this suite of rock.

3.5. Trachytic breccia

The trachytic breccia is light-grey or yellow brown with fine-grained porphyritic and cryptoexplosive breccia structure. Tabular sanidine occurs as phenocryst with fine sanidine and biotite forming the matrix. The rock contains abundant breccias of various compositions, sizes and irregular shapes such as sandstone, nepheline syenite and diopside syenite. Further geochemical work of this suite of rock is hindered due to the severe weathering and the abundant breccias.

3.6. Pseudoleucite phonolitic breccia

Pseudoleucite phonolitic breccia outcrops in the center of the complex. It is dark-brown in color, cryptoexplosive breccia structure and porphyritic with phenocrysts of pseudoleucite and sanidine, the pseudoleucite which keeps the crystal shape of leucite is usually composed of aggregates of nepheline and orthoclase. The matrix is composed of orthoclase and biotite. Like the trachytic breccia, the pseudoleucite phonolitic breccia also contains breccias of almost all rock types of this complex and suffered extensive and severe weathering, thus is also hard to carry out further geochemical investigation as the trachytic breccia.

4. Analytical methods

Mineral compositions were analyzed in the Institute of Geology and Geophysics (IGG), Chinese Academy of Sciences using a Cameca SX51 electron microprobe. The operating conditions were: 15 kV accelerating voltage, 20 nA beam current. A PAP matrix correction program was used in data processing (Pouchou and Pichoir, 1991). Natural and synthetic mineral standards were applied for calibration.

Fresh samples selected for bulk rock major, trace element and isotopic analyses were crushed in a ceramic jaw crusher. The resulting small fragments were hand-picked and rinsed with distilled water and then ground to powder (ca. 200 mesh) in an agate mortar. Major elements were determined on the fused glass discs by X-ray fluorescence spectroscopy (XRF) with a Shimadzu XRF 1500 sequential spectrometer at the IGG. The analytical uncertainties are generally within 1–5%. Loss on ignition (LOI) was determined by routine procedures. Trace element abundances were measured by the inductively coupled plasma mass spectrometry (ICP-MS) at IGG using a Finnigan MAT Element spectrometer, which has a good stability range of 5% for most elements.

Sr and Nd isotopic ratios were measured using a Finnigan MAT262 thermal ionization mass spectrometer (TIMS) housed in the Laboratory for Radiogenic Isotope Geochemistry, IGG. Static multi-collection mode was used during the measurement. Traditional cation exchange technique was adopted for chemical separation. The isotopic ratios were corrected for mass fractionation by normalizing to $^{86}Sr/^{88}Sr=0.1194$ and $^{146}Nd/^{144}Nd=0.7219$ respectively. Long-term laboratory measurements of the La Jolla Nd and SRM 987 Sr standards yield $^{143}Nd/^{144}Nd=0.511861\pm9$ (2σ) and $^{87}Sr/^{86}Sr=0.710255\pm7$ (2σ). Pb was separated by anion exchange technique with diluted HBr as an eluant.

Please cite this article as: Ying, J. et al. Petrology and geochemistry of Zijinshan alkaline intrusive complex in Shanxi Province, western North China Craton: Implication for magma mixing of different sources in an extensional regime. Lithos (2007), doi:10.1016/j.lithos.2007.02.001

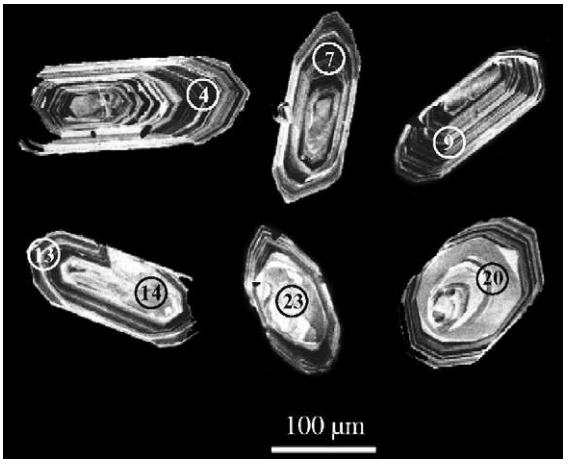


Fig. 2. Representative cathodoluminescence images of zircon grains from the monzonite, Zijinshan complex. The numbers correspond to the spots in Table 1.

Isotopic ratios were also measured with the Finnigan MAT262 mass-spectrometer in IGG, repeated analyses of NBS 981 yield $^{204}Pb/^{206}Pb = 0.05897 \pm 15$, $^{207}Pb/^{206}Pb = 0.91445 \pm 80$, $^{208}Pb/^{206}Pb = 2.16170 \pm 180$.

Laser ablation techniques were used in zircon age determination. The analyses were conducted with an Elan 6100 DRC ICPMS equipped with 193 nm Excimer laser, which is housed in the Department of Geology, Northwest University, Xi'an, China. Zircon 91500 was used as a standard, spot size is 30 μm. Raw data was reduced using the GLITTER program. Detailed analytical procedures were described by Yuan et al. (2004).

In-situ zircon Hf isotopic compositions were determined using the Neptune MC-ICPMS, which attached with a 193 nm ArF excimer laser at IGG. Spot size of 63 μm and laser repetition rate of 10 Hz with pulse energy of 100 mJ/pulse were used during the analyses. Detailed instrumental conditions, data acquisition, calibration and isobaric interference correction were described by Wu et al. (2006).

5. Results

5.1. Geochronology

Zircons are abundant in monzonite, but rare in other types of rocks. We are unable to extract zircons from

Table 1
Laser ablation ICP-MS U–Pb data of zircons in the monzonite from the Zijinshan complex

Spot	$^{232}Th/^{238}U$	Isotopic ratio						Age (Ma)	
		$^{207}Pb/^{206}Pb$	1σ	$^{207}Pb/^{235}U$	1σ	$^{206}Pb/^{238}U$	1σ	$^{206}Pb/^{238}U$	1σ
Rim									
1	0.68	0.0887	0.0021	0.2281	0.0094	0.0188	0.0003	120.1	1.9
2	0.78	0.0913	0.0034	0.2345	0.0083	0.0188	0.0003	120.1	1.7
3	0.78	0.0501	0.0021	0.1303	0.0052	0.0191	0.0003	122.0	1.6
4	0.57	0.0579	0.0024	0.1556	0.0062	0.0194	0.0003	124.1	1.6
5	0.78	0.0568	0.0017	0.1577	0.0047	0.0201	0.0002	128.3	1.5
6	0.46	0.0491	0.0040	0.1353	0.0108	0.0201	0.0004	128.4	2.4
7	0.84	0.0536	0.0035	0.1492	0.0095	0.0202	0.0003	128.7	2.1
8	0.48	0.0634	0.0047	0.1774	0.0127	0.0202	0.0004	129.1	2.5
9	1.05	0.0614	0.0032	0.1701	0.0086	0.0204	0.0003	130.0	2.1
10	0.46	0.0450	0.0024	0.1261	0.0065	0.0206	0.0003	131.6	1.9
11	0.71	0.0474	0.0023	0.1331	0.0062	0.0207	0.0003	131.9	1.9
12	0.46	0.0492	0.0004	0.1354	0.0107	0.0202	0.0004	128.5	2.3
13	0.83	0.0534	0.0034	0.1492	0.0095	0.0202	0.0003	128.8	2.0
Core									
14	0.39	0.1244	0.0021	4.9621	0.0805	0.2868	0.0031	1625.5	15.5
15	0.30	0.1236	0.0019	5.5158	0.0801	0.3221	0.0034	1800.1	16.5
16	0.26	0.1178	0.0013	5.2277	0.0545	0.3222	0.0031	1800.4	15.3
17	0.67	0.1045	0.0025	4.6255	0.1053	0.3223	0.0039	1801.0	19.4
18	0.30	0.1231	0.0014	4.8014	0.0546	0.2841	0.0028	1612.0	14.1
19	0.54	0.1128	0.0016	4.8593	0.0659	0.3154	0.0033	1767.0	15.9
20	0.32	0.1229	0.0026	5.6173	0.1137	0.3349	0.0041	1862.0	19.9
21	0.48	0.1071	0.0015	4.7029	0.0617	0.3223	0.0033	1801.2	16.1
22	0.20	0.0993	0.0012	4.2385	0.0481	0.3141	0.0031	1760.6	15.2
23	0.30	0.0979	0.0012	4.2957	0.0509	0.3229	0.0032	1803.7	15.6
24	0.35	0.0964	0.0015	4.6105	0.0695	0.3522	0.0037	1945.1	17.9

Please cite this article as: Ying, J. et al. Petrology and geochemistry of Zijinshan alkaline intrusive complex in Shanxi Province, western North China Craton: Implication for magma mixing of different sources in an extensional regime. Lithos (2007), doi:10.1016/j.lithos.2007.02.001

other types of rocks. Zircons in the monzonites are euhedral and range up to 100 micron in size, most of them are transparent and light brown in color and have oscillatory zoning. Some grains are zoned with apparently rounded or irregular cores mantled by euhedral overgrowths which also have oscillatory zoning (Fig. 2).

The zircon U–Pb data were presented in Table 1 and Fig. 3. Analyses of zircon grains with oscillatory structure are concordant or near concordant and yield a weighted mean $^{206}Pb/^{238}U$ age of 127.2±2.7 Ma (n=9) (Fig. 3b). This age is interpreted as crystallization age of the monzonite. The zircon cores, most of which are discordant, yield a much older $^{206}Pb/^{238}U$ upper intercept age of 1827±100 Ma or $^{207}Pb/^{206}Pb$ age of 1821±120 Ma (Fig. 3a). This age is quite similar to the age of zircons of metamorphic origin from the basement rocks in this region (Zhao et al., 2002), thus we interpret this age as a metamorphic age for inherited zircons.

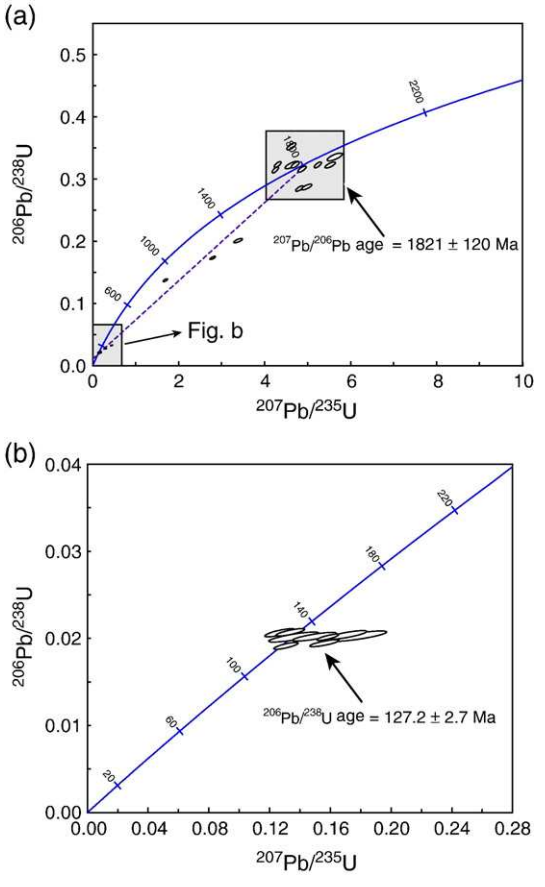


Fig. 3. Zircon U–Pb concordia diagram for the monzonite. The zircon cores give a mean $^{207}Pb/^{206}Pb$ age of 1.8 Ga (a), while the rims yield a $^{206}Pb/^{238}Pb$ age of 127 Ma (b).

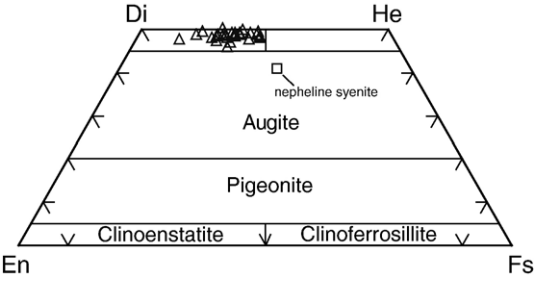


Fig. 4. Classification of pyroxene from the Zijinshan alkaline complex (after Morimoto, 1988). Note that the pyroxene from the nepheline syenite falls into the augite field.

5.2. Mineral chemistry

5.2.1. Pyroxene

Pyroxene is the most abundant mafic minerals in the Zijinshan complex. All pyroxenes except those from the nepheline syenite can be classified as diopside (Morimoto, 1988). The pyroxene from the nepheline syenite is augite due to its lower CaO content (Fig. 4). The diopside from the diopside syenite shows zoned texture in which the core is richer in MgO than the rim (Table 2). Generally, the diopside from the diopside syenite has higher MgO content than those from the monzonite and the nepheline syenite.

5.2.2. Amphibole

Amphibole in the monzonite occurs in small amounts along the cleavage of the diopside, while in the diopside syenite, anhedral amphibole occurs abundantly. All amphiboles belong to the sodic–calcic group ($Ca+Na \geq 1$ and $0.5<Na<1.5$) according to the classification of Leake et al. (1997) (Table 2). The amphiboles from the monzonite and the diopside syenite can be further classified as magnesiokatophorite ($6.5<Si<7.5$ and $Mg^{\#}>0.5$) and taramite ($5.5<Si<6.5$ and $Mg^{\#}<0.5$), respectively based on their Si and $Mg^{\#}$ ($Mg/(Mg+Fe^{2+})$).

5.2.3. Nepheline

Nepheline occurs almost in all rocks except the monzonite, and is commonly replaced by other feldspathoids such as sodalite. The nepheline is homogeneous with end-member composition of $Ne_{70}Ks_{28}Q_2$.

5.2.4. Feldspars

Plagioclase only occurs in the monzonite. It is homogeneous and belongs to andesine with its composition of $Ab_{64}An_{32}Or_4$. Alkali feldspar occurs in all types of rocks. The alkali feldspar in the monzonite is more sodic than those from the other rocks with end-member composition of $Ab_{45}Or_{52}An_3$. The orthoclase

Please cite this article as: Ying, J. et al. Petrology and geochemistry of Zijinshan alkaline intrusive complex in Shanxi Province, western North China Craton: Implication for magma mixing of different sources in an extensional regime. Lithos (2007), doi:10.1016/j.lithos.2007.02.001

Table 2
Representative electron microprobe analyses of minerals from Zijinshan complex

	Pyroxene						Amphibole			Biotite	
	1	1	2	2	2	3	1	2	2	3	3
Sample	ZJS01	ZJS02	ZJS03-c	ZJS03-r	03ZJS07	ZJS08	ZJS01	ZJS03	ZJS17	ZJS-08	ZJS15
SiO_2	51.8	50.9	53.1	47.7	49.4	52.7	45.3	39.0	38.7	36.1	35.8
TiO_2	0.20	0.28	0.33	1.14	0.77	0.10	0.63	2.58	2.74	2.40	2.88
Al_2O_3	0.95	1.58	1.09	3.95	3.05	0.49	6.57	11.4	11.7	8.99	9.80
FeO	9.98	9.58	5.47	14.0	10.2	16.8	14.7	19.2	19.4	27.8	24.4
Cr_2O_3	0.05	0.03	0.04	n.d.	0.03	0.02	0.09	0.01	n.d.	0.06	0.12
MnO	0.62	0.36	0.12	0.38	0.45	0.71	0.99	0.55	0.55	1.45	1.53
MgO	11.8	12.4	15.8	8.86	11.3	7.71	12.9	8.30	8.45	9.84	11.2
CaO	23.4	23.7	24.3	21.9	23.2	16.8	11.7	11.6	11.4	n.d.	n.d.
Na_2O	0.57	0.75	0.32	1.42	1.01	4.46	2.16	2.31	2.47	0.07	0.12
K_2O	n.d.	0.03	0.02	0.02	n.d.	0.03	1.14	2.09	2.11	9.59	9.83
Total	99.4	99.6	100.6	99.4	99.5	99.8	96.1	97.0	97.6	96.3	95.7
	Cations to 6 oxygens						Cations to 23 oxygens			Cations to 22 oxygens	
Si	1.957	1.933	1.951	1.854	1.887	1.985	6.86	6.09	5.995	5.79	5.70
Al^{IV}	0.043	0.067	0.049	0.146	0.113	0.015	1.14	1.91	2.005	1.70	1.84
Al^{VI}	0.000	0.004	0.000	0.035	0.025	0.007	0.03	0.19	0.139		
Fe^{2+}	0.243	0.304	0.168	0.456	0.327	0.200	1.56	2.37	2.246	3.73	3.25
Fe^{3+}	0.072	0.000	0.000	0.000	0.000	0.330	0.30	0.14	0.271		
Ti	0.006	0.008	0.009	0.033	0.022	0.003	0.07	0.30	0.319	0.29	0.35
Cr	0.001	0.001	0.001	–	0.001	0.001	0.01	0.00	–	0.01	0.02
Mg	0.667	0.702	0.868	0.514	0.645	0.433	2.90	1.93	1.954	2.35	2.67
Mn	0.020	0.012	0.004	0.013	0.015	0.023	0.13	0.07	0.072	0.20	0.21
Ca	0.949	0.965	0.955	0.917	0.950	0.678	1.90	1.93	1.900	–	–
Na	0.042	0.055	0.023	0.107	0.075	0.326	0.63	0.70	0.741	0.02	0.04
K	–	0.001	0.001	0.001	–	0.001	0.22	0.42	0.417	1.96	2.00

	Nepheline		Orthoclase				Plagioclase		Melanite	
	3	3	1	2	3	2	1	1	3	3
	ZJS08	ZJS15	ZJS02	ZJS03	ZJS15	ZJS17	ZJS01	ZJS02	ZJS08	ZJS15
SiO_2	41.9	41.2	63.9	64.7	65.5	65.6	59.7	58.6	32.5	35.3
TiO_2	n.d.	n.d.	0.14	0.13	0.05	0.09	n.d.	n.d.	7.24	1.50
Al_2O_3	32.6	32.6	18.7	19.1	18.2	18.5	24.4	24.4	0.65	0.86
FeO	1.77	1.34	0.31	0.28	0.09	0.08	0.47	0.48	23.6	26.7
MnO	n.d.	n.d.	n.d.	n.d.	n.d.	n.d.	0.01	0.01	0.48	0.47
MgO	0.01	0.21	0.01	n.d.	n.d.	n.d.	0.02	0.01	0.31	0.03
CaO	n.d.	0.04	0.50	0.22	0.04	0.20	6.53	7.59	32.3	33.8
Na_2O	15.2	15.4	4.90	2.99	0.11	3.34	7.16	6.62	0.17	0.02
K_2O	8.39	8.06	8.69	11.9	16.8	11.9	0.65	0.44	0.01	0.02
Total	99.9	98.8	97.2	99.3	100.8	99.7	98.9	98.1	97.2	98.6
	Cations to 8 oxygens								Cations to 12 oxygens	
Si	2.050	2.034	2.968	2.973	3.008	2.996	2.694	2.673	2.945	3.174
Al	1.877	1.898	1.025	1.034	0.985	0.995	1.296	1.308	0.069	0.091
Ti	–	–	0.005	0.005	0.002	0.003	0.000	0.000	0.494	0.102
Fe	0.065	0.050	0.012	0.011	0.003	0.003	0.018	0.018	1.791	2.008
Mg	0.001	0.015	0.001	–	–	–	0.001	0.001	0.041	0.004
Mn	–	–	–	–	–	–	0.000	0.000	0.037	0.036
Ca	–	0.000	0.025	0.011	0.002	0.010	0.316	0.371	3.134	3.261
Na	1.442	1.475	0.442	0.266	0.010	0.296	0.627	0.585	0.029	0.003
K	0.523	0.508	0.515	0.699	0.981	0.691	0.037	0.025	0.001	0.003

1: monzonite; 2: diopside syenite; 3: nepheline syenite; c: core, r: rim, n.d.: undetected.

Please cite this article as: Ying, J. et al. Petrology and geochemistry of Zijinshan alkaline intrusive complex in Shanxi Province, western North China Craton: Implication for magma mixing of different sources in an extensional regime. Lithos (2007), doi:10.1016/j.lithos.2007.02.001

Table 3
Major element compositions (wt.%) of samples from the Zijinshan complex

	03ZJS01	ZJS01	ZJS02	ZJS02 dupl.	ZJS03	ZJS03 dupl.	03ZJS 06	03ZJS 07	03ZJS09
Rock	Monzonite				Diopside syenite				Ne-bearing
SiO_2	61.4	59.6	58.2	58.3	52.8	53.3	53.5	53.5	53.0
TiO_2	0.46	0.59	0.78	0.79	0.92	0.99	0.98	0.97	0.97
Al_2O_3	17.9	18.1	16.5	16.6	13.8	13.9	15.7	15.6	14.6
Fe_2O_3	5.19	4.96	6.17	6.17	9.58	9.86	8.31	8.21	9.51
MnO	0.07	0.14	0.16	0.16	0.17	0.17	0.17	0.19	0.17
MgO	1.02	0.92	1.6	1.59	3.64	3.51	1.82	1.60	3.02
CaO	3.79	4.26	5.3	5.28	7.79	7.73	5.24	4.94	7.12
Na_2O	4.78	6.18	5.15	5.07	3.49	2.6	4.40	4.59	2.88
K_2O	3.89	4.25	5.35	5.34	6.01	6.07	8.43	8.60	6.86
P_2O_5	0.21	0.21	0.22	0.22	0.61	0.62	0.31	0.28	0.56
LOI	0.95	0.77	0.38	0.37	0.63	0.60	0.65	0.87	0.53
Total	99.7	99.9	99.9	99.9	99.5	99.4	99.5	99.4	99.2
	03ZJS13	03ZJS12	ZJS15	ZJS15 dupl.	ZJS08	GSR-1	GSR-1 refer.	GSR-3	GSR-3 refer.
	Ne-bearing	Nepheline syenite							
SiO_2	55.0	55.3	51.4	51.2	53.2	72.9	72.8	44.5	44.6
TiO_2	0.91	0.55	1.15	1.16	0.81	0.29	0.28	2.33	2.37
Al_2O_3	15.5	19.0	18.1	18.1	18.2	13.3	13.4	13.8	13.8
Fe_2O_3	8.88	4.06	5.16	5.25	4.63	2.12	2.14	13.3	13.4
MnO	0.16	0.08	0.11	0.11	0.11	0.06	0.06	0.17	0.17
MgO	2.52	0.47	0.69	0.69	0.81	0.41	0.42	7.76	7.77
CaO	7.12	2.48	4.79	4.80	4.46	1.51	1.55	8.73	8.81
Na_2O	3.29	4.25	5.05	5.09	2.54	3.03	3.13	3.48	3.38
K_2O	5.03	12.1	11.9	11.8	12.4	4.29	5.01	2.32	2.32
P_2O_5	0.51	0.16	0.16	0.15	0.10	0.09	0.09	0.94	0.95
LOI	0.43	1.18	1.92	1.90	2.26	0.70	0.69	2.45	2.24
Total	99.4	99.6	100.5	100.3	99.4	99.3	99.6	99.9	99.8

dupl.: duplicate analyses, refer.: recommended value for reference standard. GSR1 and GSR3 are Chinese granite and basalt standards, respectively.

from the nepheline syenite has a composition of Ab_1Or_{99}, while those in diopside syenite are characterized with $Ab_{27}Or_{72}An_1$.

5.2.5. Garnet

Garnet can be found in the nepheline syenite by forming aggregates or clots. They belong to Ti-rich (1.5–10.7 wt.% TiO_2) andradite and can be named as melanite, which is consistent with its usual association with alkaline rocks (Cooper and Reid, 1998; Gwalani et al., 2000).

5.3. Whole rock geochemistry

5.3.1. Major and trace element geochemistry

Major and trace element data are presented in Tables 3 and 4. In general, the rocks have a large variation in SiO_2 (51 wt.% for the nepheline syenite and 60 wt.% for the monzonite), they have high alkali contents with (K_2O+Na_2O) >9 wt.%, and are plotted in alkaline or peralkaline fields in an alkalinity vs. SiO_2 diagram (Fig. 5). All samples except monzonites have higher K_2O than Na_2O contents. The majority of rocks are SiO_2-undersaturated with the occurrence of modal nepheline except the SiO_2-saturated monzonite. All rocks have low MgO contents, suggesting their crystallization from highly evolved magmas.

Monzonite, diopside syenites and nepheline-bearing diopside syenites have very similar REE patterns. They are characterized with LREE enrichment and have high LREE/HREE ratios without Eu anomalies (Fig. 6). The total REE abundances of the above three type rocks range from 166 to 255 ppm with $(La/Yb)_n = 11–20$. The above-mentioned characteristics are similar to those of the Mesozoic monzonite and quartz monzonite distributed in the southern Taihang region but higher than Cretaceous gabbroic rocks in the same region (Chen et al., 2004; Wang et al., 2006). Nepheline syenite exhibits weak convex-up REE patterns with the peak at Nd.

All samples have similar trace element features as shown in the spidergrams (Fig. 7). They are characterized by HFSE depletion with larger depletion occurred

Please cite this article as: Ying, J. et al. Petrology and geochemistry of Zijinshan alkaline intrusive complex in Shanxi Province, western North China Craton: Implication for magma mixing of different sources in an extensional regime. Lithos (2007), doi:10.1016/j.lithos.2007.02.001

Table 4
Trace element concentrations (ppm) of samples from the Zijinshan complex

	03ZJS01	03ZJS01 dupl.	ZJS01	ZJS02	ZJS03	03ZJS06	03ZJS07	03ZJS07 dupl.	03ZJS09	03ZJS13	03ZJS12	ZJS15	ZJS08
	Monzonite				Diopside syenite				Ne-bearing syenite		Nepheline syenite		
V	66.4	62.9	107	139	259	274	263	260	274	215	156	318	304
Cr	74.9	79.4	4.68	3.67	14.1	67.7	54.3	53.2	73.4	62.4	65.4	4.10	5.66
Co	4.93	4.84	5.56	10.7	26.1	18.4	16.7	16.6	23.9	20.1	6.92	8.58	9.75
Ni	16.6	12.7	2.70	2.84	11.5	3.57	2.83	3.98	9.51	6.77	2.75	1.93	1.76
Cu	5.17	4.29	5.07	26.4	67.5	87.3	99.2	97.4	61.5	115	105	128	152
Zn	34.2	32.9	61.8	105	90.5	82.6	94.9	91.3	86.4	79.2	35.8	45.3	51.3
Rb	53.1	52.5	62.2	118	146	211	202	190	146	99.5	175	293	323
Sr	1278	1256	1891	1607	1807	2166	2183	2098	2168	1702	1569	833	796
Ba	1380	1318	1433	1190	1506	1576	1418	1409	1688	1258	1440	264	550
La	43.2	43.9	62.4	41.3	36.1	32.2	39.8	37.9	32.6	35.9	10.8	13.4	8.49
Ce	80.2	80.7	106	79.9	70.4	63.8	74.0	72.2	63.9	69.5	23.0	35.1	24.8
Pr	9.78	9.63	12.5	10.2	9.35	8.31	9.46	9.10	8.59	9.32	3.78	6.37	4.78
Nd	36.5	36.5	46.1	41.3	37.6	33.4	38.6	37.5	36.4	37.2	18.9	33.1	27.0
Sm	6.52	6.56	7.79	7.80	7.90	7.65	8.09	7.84	7.78	7.48	5.21	10.2	7.85
Eu	2.07	2.02	2.55	2.38	2.43	2.46	2.62	2.55	2.44	2.41	1.77	3.08	2.41
Gd	5.10	5.04	6.48	6.61	6.75	6.62	7.49	7.47	6.57	6.88	5.03	9.45	7.50
Tb	0.72	0.70	0.92	0.94	0.94	0.96	1.09	1.06	0.93	0.96	0.74	1.38	1.10
Dy	3.96	3.89	4.48	4.85	4.81	4.77	5.65	5.58	4.64	4.93	3.93	6.95	5.65
Ho	0.77	0.80	0.87	0.97	0.93	0.90	1.05	1.03	0.87	0.94	0.71	1.25	1.04
Er	2.10	2.16	2.24	2.45	2.32	2.26	2.64	2.58	2.11	2.32	1.72	3.02	2.53
Tm	0.32	0.33	0.32	0.34	0.32	0.33	0.37	0.37	0.30	0.33	0.24	0.41	0.34
Yb	2.10	2.04	2.09	2.18	2.02	1.97	2.14	2.26	1.82	2.04	1.55	2.47	2.13
Lu	0.34	0.34	0.31	0.33	0.29	0.31	0.34	0.35	0.28	0.33	0.23	0.36	0.30
Y	20.0	19.5	21.2	24.0	22.8	22.2	23.9	23.6	21.0	22.3	17.7	32.0	24.5
Nb	12.7	12.5	17.4	13.0	10.1	11.0	13.2	13.8	7.90	11.1	3.64	2.80	2.51
Ta	0.70	0.70	1.04	0.80	0.61	0.73	0.77	0.74	0.57	0.72	0.24	0.34	0.26
Zr	170	157	179	196	145	179	228	227	116	132	96.7	116	85.0
Hf	4.40	4.20	5.24	5.14	4.15	4.95	6.14	6.12	3.53	3.90	2.97	4.19	3.25
Th	5.74	5.76	9.73	6.28	4.36	5.60	7.58	7.30	2.81	2.94	1.70	1.18	0.89
U	1.24	1.22	1.44	1.29	1.21	1.17	2.36	2.33	0.84	0.59	0.64	0.54	0.42
Pb	4.17	4.02	12.2	13.0	13.1	11.3	18.4	18.5	11.6	10.4	1.94	2.60	6.76
∑REE	193.6	194.6	255.2	201.6	182.1	166.0	193.3	187.7	169.2	180.5	77.6	126.6	95.9
$(La/Yb)_n$	14.3	14.5	20.7	13.1	12.4	11.3	12.8	12.1	12.4	12.2	4.8	3.8	2.8
Eu/Eu*	1.1	1.1	1.1	1.0	1.0	1.0	1.0	1.0	1.0	1.0	1.0	1.0	1.0

dupl.: duplicate analyses, n: chondrite normalized.
$Eu/Eu^* = Eu_n/\sqrt{[(Sm)_n.(Gd)_n]}$.

in the nepheline syenite. Higher abundances of Ba, Rb and K which are characteristic mostly of feldspars are common among all rock types. Nevertheless, conspicuous Th and U depletion can also be observed in all samples except the monzonite.

5.3.2. Sr–Nd–Pb isotopes

Sr, Nd and Pb isotopic compositions are presented in Table 5. Initial isotopic ratios were calculated based on the crystallization age of monzonite obtained from the zircon U–Pb analyses. The monzonite have the highest initial $^{87}Sr/^{86}Sr$ ratios (0.7051–0.7052) and the lowest $\varepsilon_{Nd}(t)$ (−9.0–−11.6) among all rock types. Diopside syenite and nepheline-bearing diopside syenite have higher $\varepsilon_{Nd}(t)$ (−7.8–−3.5) and lower $(^{87}Sr/^{86}Sr)_i$ (0.7043–0.7047) than those monzonites. The nepheline syenite shows primitive or slightly depleted Sr–Nd isotopic features with positive $\varepsilon_{Nd}(t)$. A general trend that the Sr and Nd isotopic compositions become more depleted from the outer to the center of the complex was illustrated in the Sr–Nd isotopic correlation diagram (Fig. 8).

All samples have positive Δ8/4 and thus fall above the North Hemisphere Reference Line (NHRL) in the $^{206}Pb/^{204}Pb$ vs. $^{208}Pb/^{204}Pb$ diagram. They scatter along the NHRL in the $^{206}Pb/^{204}Pb$ vs. $^{207}Pb/^{204}Pb$ plot (Fig. 9). The monzonite has the least radiogenic lead isotopes ($^{206}Pb/^{204}Pb$=17.85–17.97, $^{207}Pb/^{204}Pb$=15.39–15.45 and $^{208}Pb/^{204}Pb$=37.98–38.10) while the nepheline syenite has the most radiogenic lead isotopic ratios with

Please cite this article as: Ying, J. et al. Petrology and geochemistry of Zijinshan alkaline intrusive complex in Shanxi Province, western North China Craton: Implication for magma mixing of different sources in an extensional regime. Lithos (2007), doi:10.1016/j.lithos.2007.02.001

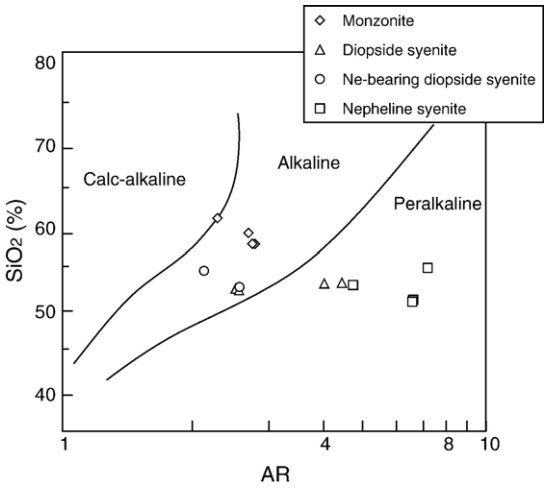


Fig. 5. AR vs. SiO_2 diagram of Wright (1969). Alkalinity ratio (AR)=$(Al_2O_3+CaO+Na_2O+K_2O)/(Al_2O_3+CaO-K_2O-Na_2O)$.

$^{206}Pb/^{204}Pb=18.57–18.81$, $^{207}Pb/^{204}Pb=15.49–15.54$ and $^{208}Pb/^{204}Pb=38.25–38.58$. Generally, all samples from the Zijinshan complex, with their high Pb isotopic compositions, show apparent contrast to the Cretaceous gabbros and Mesozoic intrusions in the Taihang regions (Chen et al., 2004; Zhang et al., 2004; Wang et al., 2006) and Cenozoic basalts in the Western Block of NCC (Tang et al., 2006).

5.4. Zircon Hf isotope

Hf isotopic compositions of zircon are listed in Table 6 and illustrated in Fig. 10. All zircons no matter the rims or the cores have very low $^{176}Lu/^{177}Hf$ ratios implying the negligible accumulation of radiogenic ^{177}Hf after zircon crystallization. The $^{176}Hf/^{177}Hf$ ratios of the zircon rims ranging from 0.282193 to 0.282335 are much higher than those of the zircon cores which have $^{176}Hf/^{177}Hf$ values

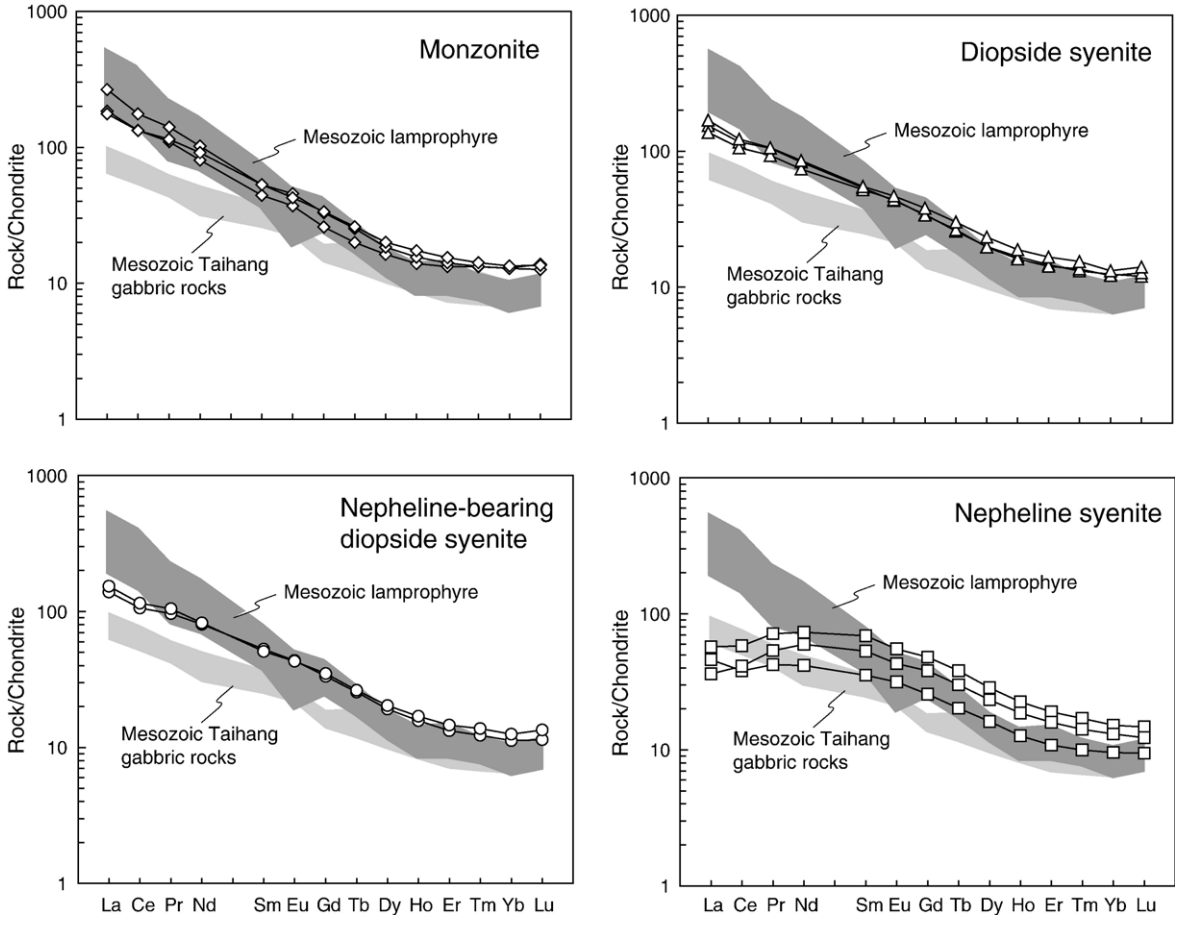


Fig. 6. Chondrite-normalized REE patterns for the Zijinshan complex. Mesozoic lamprophyres and gabbroic rocks from the Taihang region (Chen and Zhai, 2003; Wang et al., 2006) are also shown for comparison. Chondrite values are from Anders and Grevesse (1989).

Please cite this article as: Ying, J. et al. Petrology and geochemistry of Zijinshan alkaline intrusive complex in Shanxi Province, western North China Craton: Implication for magma mixing of different sources in an extensional regime. Lithos (2007), doi:10.1016/j.lithos.2007.02.001

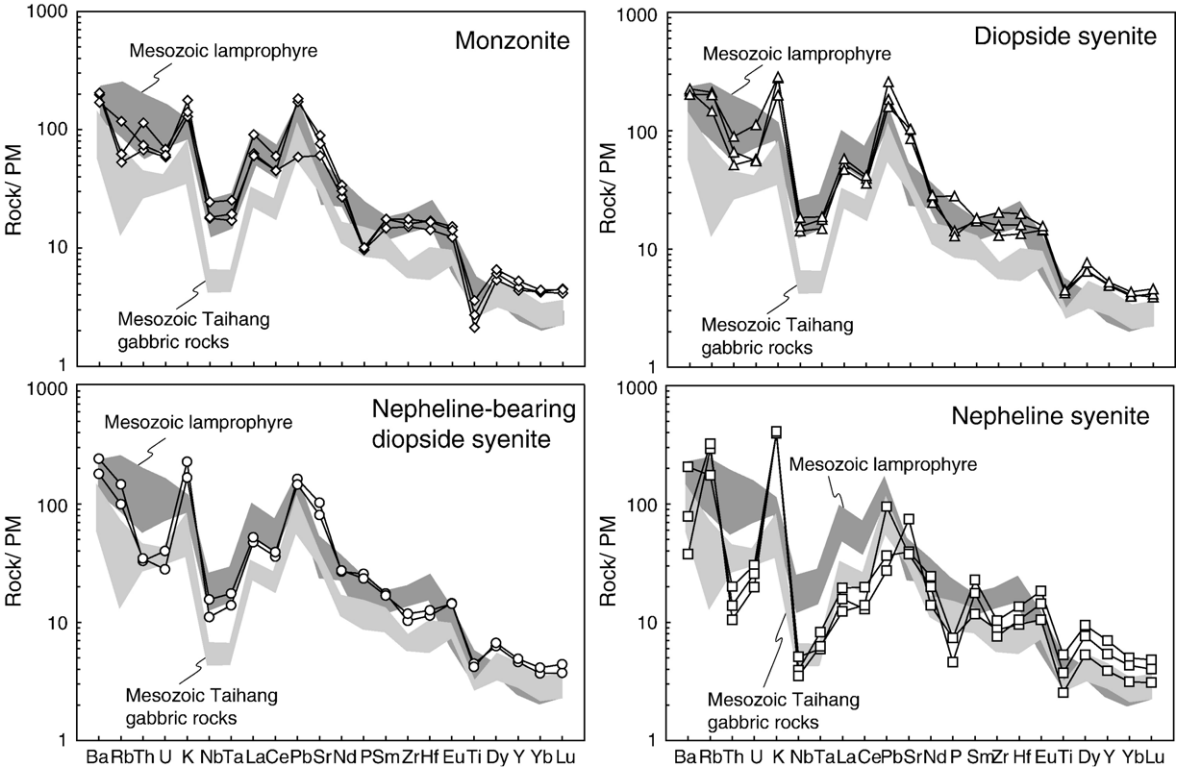


Fig. 7. Primitive mantle-normalized spidergrams for the Zijinshan complex. Mesozoic lamprophyres and gabbroic rocks from the Taihang region (Chen and Zhai, 2003; Wang et al., 2006) are also shown for comparison. Primitive mantle values are from Sun and McDonough (1989).

between 0.281509 and 0.281807. Correspondingly, the zircon rims have $\varepsilon_{Hf}(t)$ values of −12.7–−17.5 and the cores have $\varepsilon_{Hf}(t)$ of −5.8–4.4.

6. Discussion

6.1. Intrusive age and inherited zircon

Though many efforts were made to obtain the intrusive age of this complex in the past, no consistent results have been reached so far. Wu et al. (1966) firstly determined the absolute age of the complex by K–Ar method and got an age of 135 Ma. Yan et al. (1988) and Zhou et al. (1996) separately utilized Rb–Sr isochron technique for the age determination, but they got different results of 132 Ma and 153 Ma, and both of which being with very large uncertainties.

It is well known that the zircon U–Pb isotopic system can provide the most reliable age for crystalline rocks due to its highest closure temperature and strong resistance to the late stage geological processes. The apparent oscillatory zoning of the simple zircon grains and the rim portions of complex zircons from the Zijinshan intrusion revealed their magmatic origin. Thus, we interpret the age of 127 Ma as the crystallization age of the monzonite.

The rounded or irregular shape and the lack of oscillatory zoning for the cores of the complex zircons suggested that these cores are of metamorphic origin and represented inherited zircons. As introduced in the geologic background, the litho-tectonic assemblages and geochronology of the basement rocks have been well documented (Zhao et al., 2001). The basement rock of this region is composed of Late Archean to Paleoproterozoic TTG gneisses, granitoids and arc volcanic rocks. These rocks, on the one hand, preserved their protolith ages of ~2.5 Ga, and on the other hand, recorded a peak high pressure metamorphic age of 1.8 Ga which resulted from the collision between the Eastern and Western Blocks of the NCC. The age of around 1.8 Ga of the inherited zircon core from the Zijinshan monzonite is consistent with the peak metamorphic age of the basement rock of the Central Zone. Therefore, we deduce that the basement rock or lower crust rock plays an important role in the formation of the Zijinshan complex. However, the paucity of the age of 2.5 Ga in the inherited zircon contradict with the ubiquitous zircon core of 2.5 Ga in the basement rock (Zhao et al., 2001, 2002), we tentatively deem that the

Please cite this article as: Ying, J. et al. Petrology and geochemistry of Zijinshan alkaline intrusive complex in Shanxi Province, western North China Craton: Implication for magma mixing of different sources in an extensional regime. Lithos (2007), doi:10.1016/j.lithos.2007.02.001

ARTICLE IN PRESS

Table 5
Sr–Nd–Pb isotopic ratios for the Mesozoic Zijinshan complex

Sample	$^{87}Rb/^{86}Sr$	$^{87}Sr/^{86}Sr \pm 2\sigma$	$(^{87}Sr/^{86}Sr)_i$	$^{147}Sm/^{144}Nd$	$^{143}Nd/^{144}Nd \pm 2\sigma$	$(^{143}Nd/^{144}Nd)_i$	$\varepsilon_{Nd}(t)$	$^{206}Pb/^{204}Pb$	$^{207}Pb/^{204}Pb$	$^{208}Pb/^{204}Pb$
Monzonite										
03ZJS01	0.1325	0.705434±10	0.705197	0.1065	0.511970±11	0.511882	−11.6	17.972	15.441	38.099
ZJS01	0.1065	0.705276±12	0.705085	0.1044	0.512036±13	0.511949	−10.2	17.853	15.397	37.976
ZJS02	0.1965	0.705415±14	0.705064	0.1216	0.512114±12	0.512013	−9.0	17.873	15.448	37.979
Diopside syenite										
ZJS03	0.2108	0.704849±13	0.704472	0.1285	0.512282±13	0.512176	−5.8	18.180	15.448	37.972
03ZJS06	0.2735	0.704808±13	0.704319	0.1346	0.512407±11	0.512296	−3.5	18.331	15.471	38.119
03ZJS06-dupl.	0.1952	0.704854±13	0.704504	0.1332	0.512351±10	0.512240	−4.6			
03ZJS07	0.2543	0.704732±13	0.704277	0.1304	0.512394±11	0.512287	−3.7	18.321	15.475	38.115
Ne-bearing diopside syenite										
03ZJS09	0.1757	0.704760±09	0.704446	0.1316	0.512294±12	0.512185	−5.6	18.162	15.459	37.966
03ZJS13	0.1520	0.705016±12	0.704745	0.1262	0.512177±11	0.512074	−7.8	17.973	15.461	37.914
Nepheline syenite										
03ZJS12	0.2929	0.704620±14	0.704096	0.1717	0.512607±11	0.512464	−0.2	18.807	15.514	38.577
03ZJS12-dupl.	0.2987	0.704214±13	0.703679	0.1694	0.512564±12	0.512423	−1.0			
ZJS15	1.069	0.706017±09	0.704102	0.1796	0.512630±11	0.512481	0.1	18.608	15.491	38.254
ZJS08	1.310	0.706546±13	0.704200	0.1834	0.512642±11	0.512490	0.3	18.574	15.539	38.376

Initial isotopic ratios were calculated assuming an age of 127 Ma. Epsilon values are calculated using present-day ratios of $^{147}Sm/^{144}Nd=0.1967$, $^{143}Nd/^{144}Nd=0.512638$, $^{87}Rb/^{86}Sr=0.0847$, and $^{87}Sr/^{86}Sr=0.7045$ for Chondrite Uniform Reservoir (CHUR). dupl.: duplicate analyses.

Please cite this article as: Ying, J. et al. Petrology and geochemistry of Zijinshan alkaline intrusive complex in Shanxi Province, western North China Craton: Implication for magma mixing of different sources in an extensional regime. Lithos (2007), doi:10.1016/j.lithos.2007.02.001

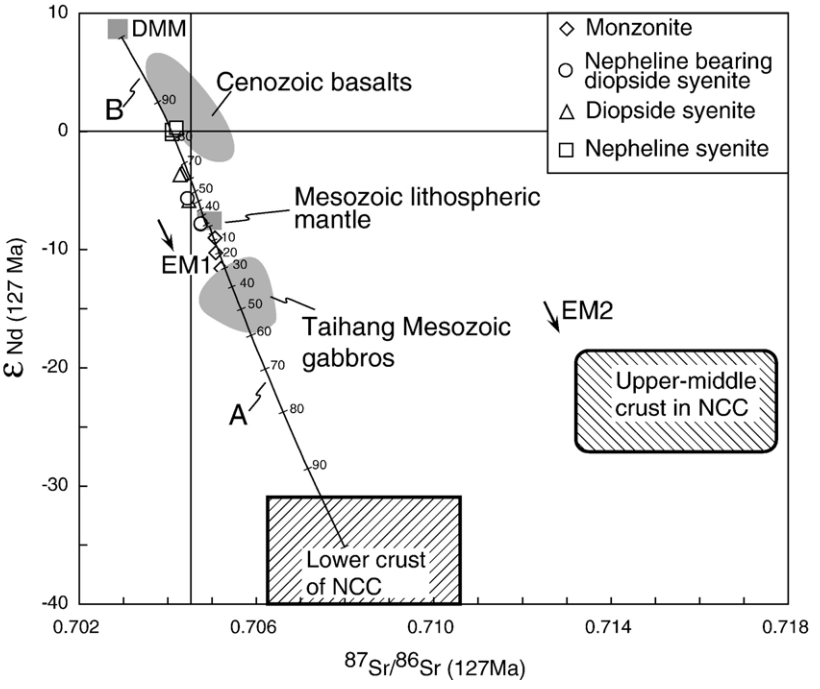


Fig. 8. Initial $^{87}Sr/^{86}Sr$ vs. ε_{Nd} (127 Ma) diagram for the Zijinshan complex. Isotopic data of the Mesozoic gabbroic rocks from the Taihang Mountains (Chen et al., 2004; Zhang et al., 2004; Wang et al., 2006) are shown for comparison. Lower crust and upper–middle crust of the NCC are from Jahn et al. (1999). The Mesozoic lithospheric mantle was defined according to Chen and Zhai (2003). Cenozoic basalts from Taihang regions are from Xu et al. (2004) and Tang et al. (2006). DMM, EM 1 and EM 2 are from Zindler and Hart (1986). The mixing modelling parameters used for lower crust of NCC are Sr=300 ppm, $^{87}Sr/^{86}Sr$=0.708, Nd=24 ppm, ε_{Nd}=−35; Sr=1000 ppm, $^{87}Sr/^{86}Sr$=0.705, Nd=70 ppm, ε_{Nd}=−8 for enriched lithospheric mantle derived melts, and Sr=150 ppm, $^{87}Sr/^{86}Sr$=0.703, Nd=15 ppm, ε_{Nd}=8 for asthenosphere-derived magma (Jahn et al., 1999; Chen and Zhai, 2003). Curve A refers to the mixing line between the enriched lithospheric mantle and the lower crust which resulted in the formation of the monzonite. Curve B is the mixing line between the depleted asthenosphere and the enriched lithospheric mantle which can account for the formation of diopside syenite and nepheline syenite.

basement rock involving the formation of the Zijinshan complex experienced high grade metamorphism and the protolithic zircons were totally substituted by the metamorphic zircons.

6.2. Petrogenesis

6.2.1. Monzonite

The monzonite has higher SiO_2 (>58 wt.%) and low MgO (<1.6 wt.%), suggesting its formation from an evolved magma, none of the samples have Eu anomalies, indicating that plagioclase fractionation did not play an important role in the evolution of the magma and may only undergo high-pressure (plagioclase absent) fractionation before its emplacement at high level. On the other hand, spatial relations provide undoubted evidence supporting that the monzonite is the earliest intrusion among the rocks from the Zijinshan complex, thus it is difficult to deem that the monzonite was produced from relative mafic rocks of later intrusion such as the diopside syenite through fractional crystallization. Partial melting experiments on the lower crust reveals that the partial melts are high in SiO_2 (>58%), Al_2O_3 (>17%) and Na_2O and low in MgO when the partial melting degree is less than 40% (Wolf and Wyllie, 1994; Rapp and Watson, 1995). The compositional similarity of the Zijinshan monzonite to the experimental melts of lower crust suggests that the lower crust do play a significant role in the formation of monzonitic magma of the Zijinshan complex (Fig. 11). The existence of inherited zircon cores also provides compelling evidence for the involvement of lower crust in the formation of monzonite.

The NCC has an Archean lower crust mainly composed of granulites (Jahn and Zhang, 1984), which might be the potential source of the Zijinshan monzonite. However the Sr–Nd isotopic compositions of the Archean granulite terrain of the NCC are quite different from those of Zijinshan monzonite. The $^{87}Sr/^{86}Sr$ values of the NCC granulite terrain range from 0.706 to 0.720 and the $\varepsilon_{Nd}(t)$

Please cite this article as: Ying, J. et al. Petrology and geochemistry of Zijinshan alkaline intrusive complex in Shanxi Province, western North China Craton: Implication for magma mixing of different sources in an extensional regime. Lithos (2007), doi:10.1016/j.lithos.2007.02.001

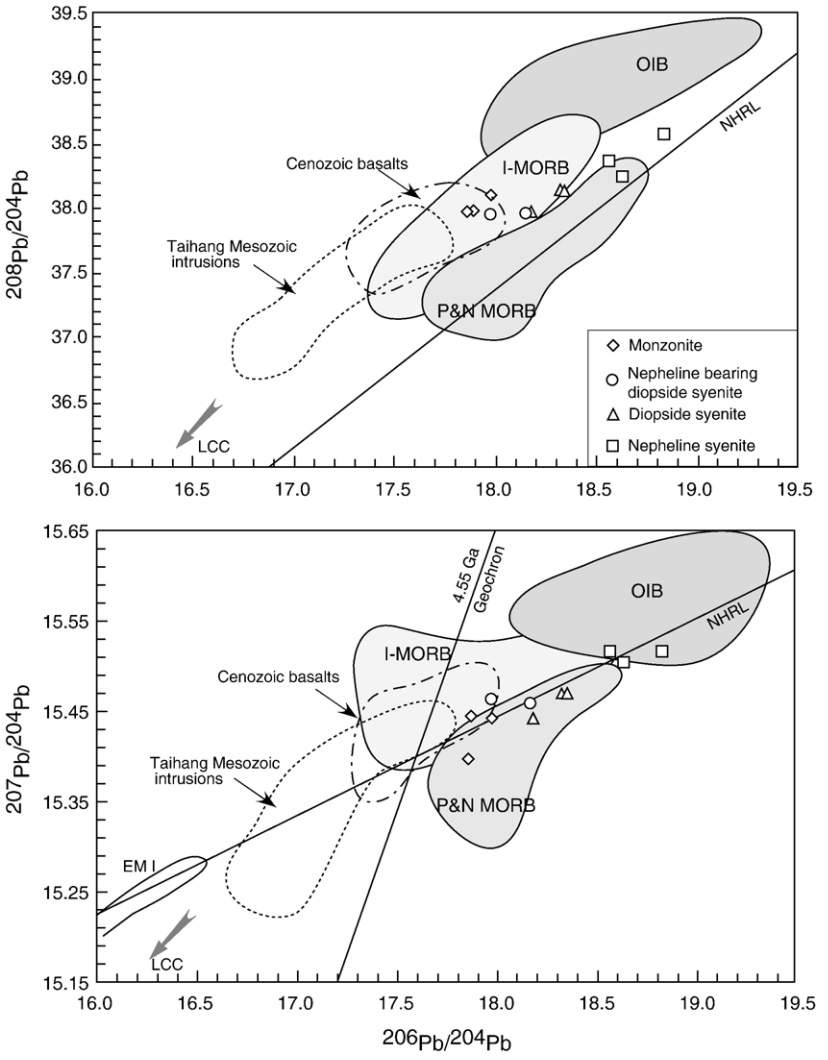


Fig. 9. $^{208}Pb/^{204}Pb$ vs. $^{206}Pb/^{204}Pb$ and $^{207}Pb/^{204}Pb$ vs. $^{206}Pb/^{204}Pb$ diagram for the Zijinshan complex. The fields for I-MORB (Indian MORB), P&N-MORB (Pacific and North Atlantic MORB), OIB, NHRL and 4.55 Ga geochron are from Hart (1984); Barry and Kent (1998) and Zou et al. (2000). Also shown are Taihang Mesozoic intrusions (Chen et al., 2004; Zhang et al., 2004; Wang et al., 2006) and Cenozoic basalts of Taihang regions (Tang et al., 2006) for comparison.

could be as low as −35 (Jahn and Zhang, 1984; Zhou et al., 2002), such values are much lower than those of the Zijinshan monzonite. Moreover, unradiogenic Pb isotopic ratios that have been generally observed in the lower crustal granulites are not the features for the Zijinshan monzonite (Fig. 9). Consequently, only the contribution of lower crust can not account for the geochemical characteristics of the Zijinshan monzonite, and a considerable amount of mantle-derived magma is required in their geneses.

Are these mantle-derived magmas originated from the asthenosphere or lithospheric mantle? Generally speaking, the asthenosphere is convective and hot and has a depleted or primitive mantle character in both chemical and isotopic compositions (MORB-like) due to the circulation of incipient melts from low degree melting. In contrast, the lithospheric mantle is relative cold and isotopically enriched due to its long history of isolation from the asthenosphere and interaction with magmas. The negative $\varepsilon_{Hf}(t)$ values of zircon rims of the monzonite implied that the magma from which the zircon crystallized are enriched in Hf isotopic composition, so the contribution of the asthenosphere which is depleted in Hf isotope ($\varepsilon_{Hf}(t)>0$) can be ruled out, and the mantle-derived magma required in monzonite geneses should originate from the lithospheric mantle.

Please cite this article as: Ying, J. et al. Petrology and geochemistry of Zijinshan alkaline intrusive complex in Shanxi Province, western North China Craton: Implication for magma mixing of different sources in an extensional regime. Lithos (2007), doi:10.1016/j.lithos.2007.02.001

Table 6
Zircon Hf isotopic compositions of monzonite, Zijinshan complex

	Spot	$^{176}Yb/^{177}Hf$	$^{176}Lu/^{177}Hf$	$^{176}Hf/^{177}Hf$	$2\sigma_m$	$\varepsilon_{Hf}(0)$	$\varepsilon_{Hf}(t)$	T_{DM1}(Ma)	T_{DM2} (Ma)	$f_{Lu/Hf}$
Rim	1	0.041744	0.001774	0.282272	0.000032	−17.7	−15.1	1412	2971	−0.95
	2	0.023379	0.001039	0.282335	0.000043	−15.4	−12.7	1295	2764	−0.97
	3	0.038500	0.001715	0.282243	0.000033	−18.7	−16.1	1451	3062	−0.95
	4	0.066131	0.002553	0.282276	0.000013	−17.6	−15.0	1436	2964	−0.92
	5	0.050705	0.002010	0.282286	0.000012	−17.2	−14.6	1401	2928	−0.94
	6	0.055276	0.002274	0.282230	0.000036	−19.2	−16.6	1491	3104	−0.93
	7	0.046845	0.001847	0.282241	0.000029	−18.8	−16.1	1458	3067	−0.94
	8	0.026666	0.001112	0.282230	0.000027	−19.2	−16.5	1445	3097	−0.97
	9	0.040793	0.001704	0.282267	0.000035	−17.9	−15.2	1416	2986	−0.95
	10	0.064098	0.002362	0.282194	0.000031	−20.4	−17.8	1546	3218	−0.93
	11	0.033082	0.001340	0.282240	0.000031	−18.8	−16.1	1440	3067	−0.96
	12	0.050064	0.002192	0.282250	0.000035	−18.5	−15.9	1460	3043	−0.93
	13	0.041553	0.001792	0.282193	0.000035	−20.5	−17.9	1525	3220	−0.95
	14	0.033454	0.001429	0.282214	0.000034	−19.7	−17.1	1481	3151	−0.96
	15	0.047748	0.002008	0.282273	0.000038	−17.6	−15.0	1419	2967	−0.94
	16	0.055164	0.002202	0.282203	0.000028	−20.1	−17.5	1527	3190	−0.93
	17	0.033338	0.001359	0.282221	0.000036	−19.5	−16.8	1468	3129	−0.96
Core	18	0.024553	0.000865	0.281512	0.000028	−44.6	−5.0	2424	3189	−0.97
	19	0.020359	0.000655	0.281628	0.000012	−40.5	−0.7	2253	2807	−0.98
	20	0.013454	0.000486	0.281638	0.000032	−40.1	−0.1	2231	2759	−0.99
	21	0.013207	0.000455	0.281620	0.000028	−40.7	−0.7	2252	2809	−0.99
	22	0.047140	0.001734	0.281504	0.000025	−44.8	−6.4	2491	3306	−0.95
	23	0.014497	0.000529	0.281445	0.000030	−46.9	−7.0	2494	3361	−0.98
	24	0.050071	0.001706	0.281807	0.000031	−34.1	4.4	2066	2364	−0.95
	25	0.021018	0.000718	0.281616	0.000030	−40.9	−1.2	2274	2852	−0.98
	26	0.014614	0.000529	0.281541	0.000025	−43.5	−3.6	2365	3065	−0.98
	27	0.022091	0.000742	0.281606	0.000030	−41.2	−1.5	2288	2884	−0.98
	28	0.019872	0.000724	0.281671	0.000029	−38.9	0.8	2199	2680	−0.98
	29	0.034410	0.001166	0.281627	0.000027	−40.5	−1.3	2285	2864	−0.96
	30	0.030908	0.000948	0.281509	0.000038	−44.7	−5.2	2433	3207	−0.97
	31	0.034786	0.001196	0.281579	0.000030	−42.2	−3.1	2353	3017	−0.96

$\varepsilon_{Hf}(t)$ for the zircon rim and core were calculated based on 127 Ma and 1821 Ma respectively. The following parameters were applied to calculation, $(^{176}Lu/^{177}Hf)_{CHUR}=0.0332$, $(^{176}Hf/^{177}Hf)_{CHUR,\ 0}=0.282772$; $(^{176}Lu/^{177}Hf)_{DM}=0.03842$, $(^{176}Hf/^{177}Hf)_{DM,\ 0}=0.28325$ (BlichertToft and Albarede, 1997; Griffin et al., 2000), ^{176}Lu decay constant $\lambda=1.867\times10^{-11}$ a^{-1} (Söderlund et al., 2004).

Previous investigation on Mesozoic lamprophyres and gabbros which were uncontaminated by crust revealed that the lithospheric mantle beneath this region are of EM-I affinity with $\varepsilon_{Nd}(135\ Ma)=-8.2$ and $(^{87}Sr/^{86}Sr)_i=0.7054–0.7058$ (Chen et al., 2003; Chen and Zhai, 2003), these values are higher than that of the monzonite and thus can be reasonably regarded as the other end-member in the monzonite origin. A simple mass balance calculation based on the Sr and Nd isotopes shows that the mixing of less than 30% lower crustal melts with lithospheric mantle derived magma can produce the observed Sr–Nd isotopic ratios of the Zijinshan monzonite (Fig. 8 curve A). Similar scenario, i.e. the involvement of lower crust was also proposed to account for the formation of the Mesozoic monzonite and quartz syenite from Aldan Shield, southeastern Siberia (Pervov et al., 1997).

Basaltic underplating into crust has been widely considered as an important mechanism to generate silicic melts in the continental crust (Atherton and Petford, 1993; Petford and Gallagher, 2001). Basaltic melts can act either as parental source or thermal trigger for crustal melting depending on the fertility of the crust, temperature and water contents of basalts (Grunder, 1995; Annen and Sparks, 2002). The geochemical features shown by Zijinshan monzonite suggest that the basaltic magma provided both material and thermal contributions to the formation of the Zijinshan monzonite.

6.2.2. Diopside syenite and nepheline-bearing diopside syenite

Several models have been proposed for the origin of syenitic magmas. Lubala et al. (1994) pointed out that the syenite may be produced by melting of crustal rocks during an influx of volatiles; syenitic magmas could also formed by partial melting of metasomatized mantle (Lynch et al., 1993) or as residual melts of differentiation of alkali basaltic magma (Brown and Becker, 1986;

Please cite this article as: Ying, J. et al. Petrology and geochemistry of Zijinshan alkaline intrusive complex in Shanxi Province, western North China Craton: Implication for magma mixing of different sources in an extensional regime. Lithos (2007), doi:10.1016/j.lithos.2007.02.001

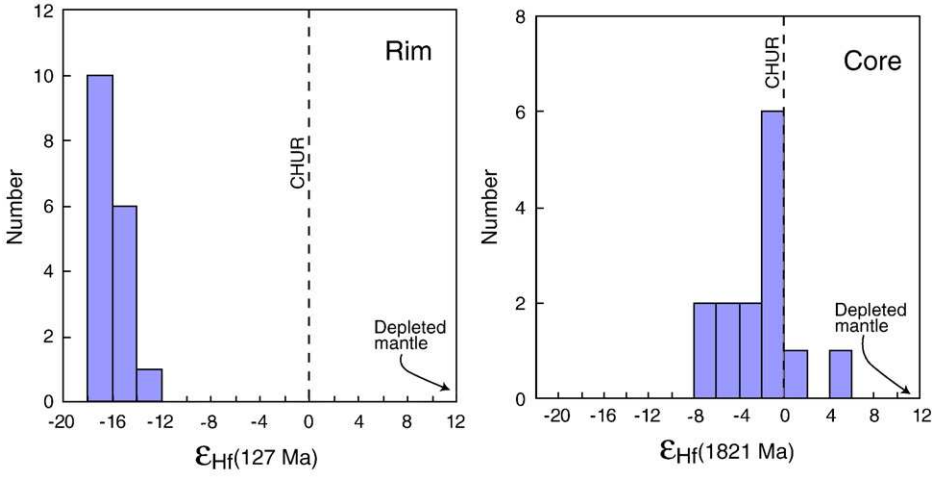


Fig. 10. Hf isotopic compositions of the zircons from the monzonite.

Litvinovsky et al., 2002). The third model for syenitic magma generation is that it may be produced through differentiation of hybrid magma formed by mixing of basaltic and silicic melts (Sheppard, 1995; Zhao et al., 1995), or by mixing of mantle derived silica undersaturated alkaline magma with granitic magma from partial melting of lower crust (Dorais, 1990).

As discussed in the origin of the monzonite, the NCC has an Archean lower crust composed dominantly of granulites, partial melts of these granulites would possess a negative Eu anomaly and low HREE due to the residual plagioclase and garnet. Both the diopside syenite and nepheline-bearing diopside syenite have relative high HREE abundances indicating a garnet-free source. Moreover, the silica under-saturation of the nepheline bearing diopside syenite is also inconsistent with the features of the crustal derived melts, as they are usually silica saturated or oversaturated. The significantly contrasting Sr–Nd isotopic compositions between the lower crust and syenite also ruled out the lower crust as the source for the diopside syenite and nepheline-bearing diopside syenite. Thus, a mantle origin was proposed for these two types of syenite, the extremely high LILE abundances of the syenite (Sr around 2000 ppm; Ba around 1600 ppm) are also evidence for the mantle origin of the syenite, as such characteristics were considered by some workers to be originated from fractionation of enriched lithospheric mantle derived basaltic magma (Litvinovsky et al., 2002).

As revealed from the studies of the Mesozoic lamprophyre in this region, the lithospheric mantle beneath this region are of EM-1 affinity with its $(^{87}Sr/^{86}Sr)_i$= 0.7054–0.7058 and ε_{Nd}=−8 (Chen and Zhai, 2003). Discernable higher ε_{Nd} values of these two type syenites than that of lithospheric mantle underneath this region suggest that besides the lithospheric mantle, another end-member with more depleted isotopic compositions than the lithospheric mantle must involve in the formation of the syenitic magma. We thus consider that the depleted end-member involving in the origin of the syenite is asthenospheric derivative. From the perspective of Sr–Nd isotopes, the syenites might be derived from the mixing of about 50–60% magma from depleted asthenosphere with 50–40% melts from enriched lithospheric mantle (Fig. 8).

6.2.3. Nepheline syenite

The MgO, Co, Cr and Ni in the nepheline syenite are lower than that of the diopside syenite (Fig. 12), which possibly implied that the nepheline syenite could be formed by fractional crystallization from the diopside syenitic magmas. However, the nepheline syenite with its high abundance of modal nepheline is more undersaturated in silica than the diopside syenite and nepheline-bearing diopside syenite, thus it is illogical that the silica undersaturated nepheline syenite formed through fractional crystallization from silica saturated diopside syenite. Furthermore, the highest ε_{Nd} and Pb isotopic ratios of the nepheline syenite among the Zijinshan complex also precluded such deduction. We believe that the nepheline syenite represented another magmatic pulse. The intrusion of the nepheline syenite branches into the diopside syenite and the occurrence of the diopside syenite enclaves in nepheline syenite are consistent with that the nepheline syenites are products of another magmatic activity later than diopside syenite and nepheline-bearing diopside syenite.

It is noted from the Sr–Nd correlation diagram that the nepheline syenites have homogeneous and primitive

Please cite this article as: Ying, J. et al. Petrology and geochemistry of Zijinshan alkaline intrusive complex in Shanxi Province, western North China Craton: Implication for magma mixing of different sources in an extensional regime. Lithos (2007), doi:10.1016/j.lithos.2007.02.001

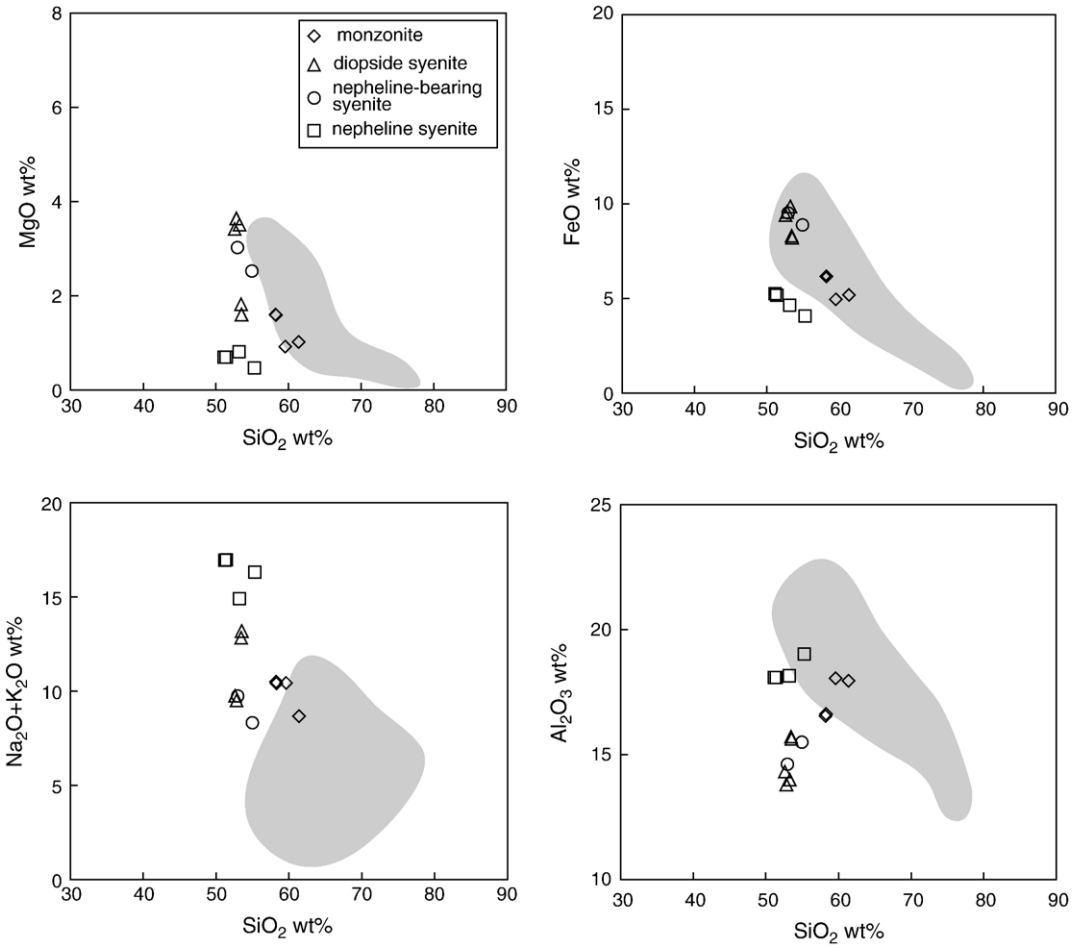


Fig. 11. Compositional comparison between the partial melts (melting degree less than 40%) of the lower crust materials and the Zijinshan complex. The shaded area refers to the experimental melts of the lower crust, experimental data are from Rapp and Watson (1995) and Wolf and Wyllie (1994).

Sr–Nd isotopic compositions which are higher than those of diopside syenite and nepheline-bearing diopside syenite and the EM-1 lithospheric mantle (Fig. 8). The Pb isotopes also point to a depleted mantle origin (Fig. 9). Thus we proposed a similar origin model for the nepheline syenite as for the diopside syenite, that is, the nepheline syenite formed from partial melting of a mixed mantle source between the depleted asthenosphere and enriched lithospheric mantle. The Sr–Nd isotopic modelling yields the contribution of about 80% depleted asthenosphere and 20% enriched lithospheric mantle to the magma source (Fig. 8 curve B).

The MgO, Ni, Cr and Co abundances in nepheline syenite are low and quite different from the primitive mantle derived melts. This implied that the melts had undergone significant crystal fractionation prior to emplacement. Considering that the diopside syenite has much higher abundance of diopside and amphibole and correspondingly higher MgO, Ni, Cr and Co, we deduce that the diopside, amphibole and more possibly the olivine are the main fractionation phases. The quite homogeneous Sr–Nd isotopic compositions of the nepheline syenite indicate that negligible crustal contamination occurred during the magma evolution.

Other features of the nepheline syenite that should be noted are the weak convex-up REE pattern as illustrated by the Nd at the peak and more depleted Nb and Ta concentrations than the other types of rocks. It has been well documented that the alkaline rocks derived from the enriched lithospheric mantle are characterized with depleted HFSE (Pervov et al., 1997; Litvinovsky et al., 2002; Zhang et al., 2005), such features were shared by all types of rocks of the Zijinshan complex. The more depleted Nb and Ta in nepheline could be inherited from its source character or derived from the fractionation of Ti-rich minerals which preferentially host these elements.

Please cite this article as: Ying, J. et al. Petrology and geochemistry of Zijinshan alkaline intrusive complex in Shanxi Province, western North China Craton: Implication for magma mixing of different sources in an extensional regime. Lithos (2007), doi:10.1016/j.lithos.2007.02.001

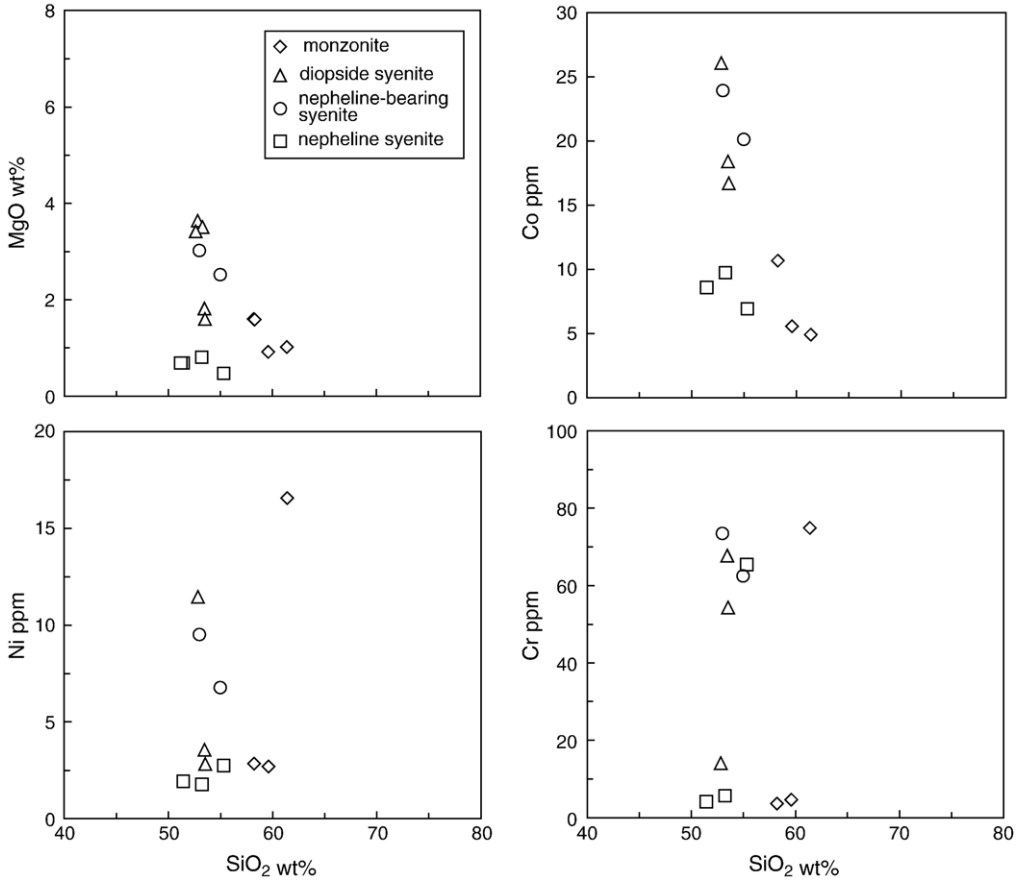


Fig. 12. Compositional variations for the different types of rocks of the Zijinshan complex.

It has been widely accepted that a number of Ti-rich minerals (titanite, rutile, ilmenite) have partition coefficients significantly greater than unity for both Nb and Ta in silicate liquids. Moreover, both rutile and titanite favor Ta with respect to the Nb and would lead to a higher Nb/Ta ratio than that in chondrite. However, In the Zijinshan complex, the Nb/Ta ratios of the nepheline syenite are lower than that of the other types of rock and the chondritic value (Fig. 13). Such a feature is inconsistent with the fractionation of the titanite or rutile from the silicate melts during the formation of the nepheline syenite. Experimental determination on partition coefficients of Nb and Ta for rutile in aqueous fluid system demonstrated that not only D_{Nb} and D_{Ta} greater than 1 but also $D_{Nb}/D_{Ta}>1$ (Green, 1995), and thus the rutile fractionation in fluid system will decrease the Nb/Ta ratios in the residues as we observed in the Zijinshan nepheline syenite. As described in the petrography section, the constituent minerals in the nepheline syenite are so coarse that some parts of the rocks have pegmatitic texture, which implies that the hydrothermal fluids played an important role in the formation of the nepheline syenite, and such a suggestion is consistent with the Nb and Ta features. We speculated that the unusual REE pattern

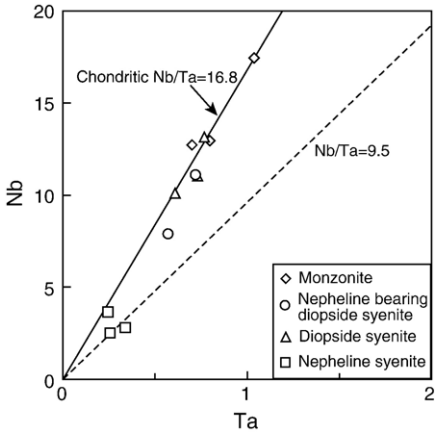


Fig. 13. Plot of whole rock Nb vs. Ta for the Zijinshan complex. Chondritic value is from Green (1995).

Please cite this article as: Ying, J. et al. Petrology and geochemistry of Zijinshan alkaline intrusive complex in Shanxi Province, western North China Craton: Implication for magma mixing of different sources in an extensional regime. Lithos (2007), doi:10.1016/j.lithos.2007.02.001

might also resulted from the influence of the hydrothermal fluids during the late stage of magma evolution though there is no reliable experimental data to describing the behavior of the REE between the Nb and Ta bearing minerals and the hydrothermal fluid.

As far as the trachytic breccia and pseudoleucite phonolitic breccia are concerned, there are several lines of evidence supporting their cryptoexplosive origin, for instance, the breccias have large variations in rock type ranging from the country rock to the alkaline rocks of each magmatic episode, the breccias varied in sizes without any sorting, the absence of volcanic explosion products such as volcanic bombs and ashes. The drilling cores as deep as 500 m show that there is no difference in lithology from the surface breccias. Moreover, the cements of the breccias are medium to fine grained, which implied their crystallization at depth.

7. Geodynamic implications

Various tectonic models have been proposed to interpret the Mesozoic magmatism in the Western Block of NCC. Being aware of the younging trend of magmatism from the coastal area to the inland of NCC and strong arc-like magma signatures of the Mesozoic magmatic rocks in the Taihang Mountains, Chen et al. (2004) proposed a continental arc model for the entire eastern China, in which the Paleo-Pacific slab subducted beneath the East Asian continent and transformed the eastern part of the NCC into an active continental margin. As a consequence, all Mesozoic magmatism is developed in a back-arc extensional setting. In this model, the fluids/melts released from the subducted slabs played a significant role in the transformation of the lithospheric mantle beneath the NCC. However, the late Mesozoic was a period when the Izanagi plate primarily moved toward the north or north-northeast, thereby giving little chance for inducing broad backarc extension in this region (Maruyama and Send, 1986; Kimura et al., 1990). Recent U–Th disequilibrium studies of the Cenozoic potassium basalts from northeastern China also argued against the material contributions from the Paleo-Pacific plate (Zou et al., 2003). Since the Taihang region is even further away from the subduction zone, thus the subduction of Pacific plate underneath the East Asia may not play an important role in the activation of the Mesozoic magmatism in the Taihang region as previously thought.

Based on the investigation of early Cretaceous gabbroic rocks from the Taihang Mountains, Wang et al. (2006) proposed that the enriched lithospheric mantle sources for the Mesozoic Taihang gabbroic rocks were formed through metasomatism by SiO_2-rich melts released from the Paleoproterozoic subducted slabs during the amalgamation of the NCC rather than the fossil Paleo-Pacific slabs, and the direct trigger for the intrusion of these gabbroic rocks is the post-orogenic extension of the Triassic subduction/collision beneath the northern and southern margin of the NCC. Such subduction/collision model was also applied to explain the Mesozoic alkaline rocks in the eastern part of NCC and compositional transformation of the lithospheric mantle beneath the NCC (Zhang et al., 2003). Here we speculated a post-orogenic extensional regime for the activation of the Zijinshan complex and that orogenic event may be related with the Paleozoic amalgamation of NCC with the Mongolian micro-continents as well as subsequent closure of Mongol–Okhotsk ocean.

It is well accepted that the NCC and Mongolian micro-continents amalgamated by the end of Paleozoic time, and the post-amalgamation extension was widespread as illustrated by the Triassic alkaline intrusions dated from 205 to 250 Ma (Shao et al., 2000; Yan et al., 2000) and late Triassic metamorphic core complex (Davis et al., 2001a) in the north China. During the collision of the Siberia Craton with the combined NCC and Mongolian continents and the subduction of Mongol–Okhotsk ocean, the tectonic regime was contractionary in mid to late Jurassic (Meng, 2003), and then to the post orogenic stage in the late Mesozoic with extensional setting dominating in this region. Regional field investigation in the adjacent region also shows that thrust-fault activation representative of a compressional regime ceased at the later Jurassic, and rift basins, metamorphic core complexes, indicating an extensional setting, occurred in the early Cretaceous (Zheng et al., 1996; Davis et al., 2001b). This extensional tectonic regime enables rapid upwelling of asthenosphere and induced concomitant decompressional partial melting. These partial melts underplated at the base of the lower crust along the cracks in the lithosphere which formed during the compressional stage. Variable proportion and episodic mixing of melts derived from the asthenosphere, and/or lithospheric mantle with lower crust materials generated the different lithologies of the Zijinshan complex.

8. Conclusions

1. The intrusion of Zijinshan alkaline complex took place in the early Cretaceous with the earliest emplacement of monzonite (127 Ma) in the outermost and the termination of cryptoexplosive pseudoleucite phonolitic breccia in the center.
2. Different lithologies of the Zijinshan complex reflect different magma pluses rather than evolved from a

Please cite this article as: Ying, J. et al. Petrology and geochemistry of Zijinshan alkaline intrusive complex in Shanxi Province, western North China Craton: Implication for magma mixing of different sources in an extensional regime. Lithos (2007), doi:10.1016/j.lithos.2007.02.001

ARTICLE IN PRESS

uniform magma chamber through fractional crystallization. The monzonite was produced from the mixing of melt from enriched lithospheric mantle with granitic magma derived from the lower crust. The diopside syenite and nepheline-bearing diopside syenite originated from a mixture of melts derived from depleted asthenosphere and enriched lithospheric mantle. The nepheline syenite has a similar origin as that for the diopside syenite, but with much higher contributions from the depleted mantle.

3. The Zijinshan complex was generated in an extensional environment which resulted in the upwelling of asthenosphere and intense crust–mantle interaction.

Acknowledgements

This work was supported by the Chinese Academy of Sciences (KZCX2-YW-103) and Natural Science Foundation of China (40303006 and 40534022). We are grateful to Y. Ma and Q. Mao for their assistance in electron microprobe analyses and to H. Li, X.D. Jin and C.F. Li for their kind help in the major, trace element and isotopic measurements. S. Foley and two anonymous reviewers are thanked for their constructive comments which greatly improved the paper.

References

Anders, E., Grevesse, N., 1989. Abundances of the elements: meteoritic and solar. Geochim. Cosmochim. Acta 53, 197–214.

Annen, C., Sparks, R.S.J., 2002. Effects of repetitive emplacement of basaltic intrusions on thermal evolution and melt generation in the crust. Earth Planet. Sci. Lett. 203, 937–955.

Atherton, M.P., Petford, N., 1993. Generation of sodium-rich magmas from newly underplated basaltic crust. Nature 362, 144–146.

Barry, T.L., Kent, R.W., 1998. Cenozoic magmatism in Mongolia and the origin of central and east Asian basalts. In: Flower, M.F.J., Chung, S.L., Lo, C.H., Lee, T.Y. (Eds.), Mantle Dynamics and Plate Interactions in East Asia. Geodynamics Series. American Geophysical Union, pp. 347–364.

BlichertToft, J., Albarede, F., 1997. The Lu–Hf isotope geochemistry of chondrites and the evolution of the mantle–crust system. Earth Planet. Sci. Lett. 148, 243–258.

Brown, P.E., Becker, S.M., 1986. Fractionation, hybridisation and magma-mixing in the Kialineq centre East Greenland. Contrib. Mineral. Petrol. 92, 57–70.

Chen, B., Zhai, M., 2003. Geochemistry of late Mesozoic lamprophyre dykes from the Taihang Mountains, north China, and implications for the sub-continental lithospheric mantle. Geol. Mag. 140, 87–93.

Chen, B., Jahn, B.M., Zhai, M., 2003. Sr–Nd isotopic characteristics of the Mesozoic magmatism in the Taihang–Yanshan orogen, North China Craton, and implications for Archaean lithosphere thinning. J. Geol. Soc. 160, 963–970.

Chen, B., Jahn, B.M., Arakawa, Y., Zhai, M.G., 2004. Petrogenesis of the Mesozoic intrusive complexes from the southern Taihang Orogen, North China Craton: elemental and Sr–Nd–Pb isotopic constraints. Contrib. Mineral. Petrol. 148, 489–501.

Cooper, A.F., Reid, D.L., 1998. Nepheline sövites as parental magmas in carbonatite complexes: evidence from Dicker Willem, Southwest Namibia. J. Petrol. 39, 2123–2136.

Davis, G.A., Zheng, Y., Zhang, C., Xu, B., 2001a. The Mesozoic Fengning–Longhua and Jiaoqier fault zone, North China: new interpretations of controversial structures. GSA abstracts with programs, A-49.

Davis, G.A., et al., 2001b. Mesozoic tectonic evolution of Yanshan fold and thrust belt with emphasis on Hebei and Liaoning Provinces, north China. In: Hendrix, M.S., Davis, G.A. (Eds.), Paleozoic and Mesozoic Tectonic Evolution of Central Asia: From Continental Assembly to Intracontinental Deformations. Geological Society of America, Boulder, Colorado, pp. 171–194.

Dorais, M.J., 1990. Compositional variations in pyroxenes and amphiboles of the Belknap Mountain complex, New Hampshire: evidence for origin of silica-saturated alkaline rocks. Am. Mineral. 75, 1092–1105.

Fan, W.M., et al., 2000. On and off the North China Craton: where is the Archaean keel? J. Petrol. 41, 933–950.

Fan, W.M., Guo, F., Wang, Y.J., Lin, G., Zhang, M., 2001. Post-orogenic bimodal volcanism along the Sulu orogenic belt in Eastern China. Phys. Chem. Earth, Part A Solid Earth Geod. 26, 733–736.

Gao, S., et al., 2004. Recycling lower continental crust in the North China Craton. Nature 432, 892–897.

Green, T.H., 1995. Significance of Nb/Ta as an indicator of geochemical processes in the crust–mantle system. Chem. Geol. 120, 347–359.

Griffin, W.L., O'Reilly, S.Y., Ryan, C.G., 1992. Composition and thermal structure of the lithosphere beneath South Africa, Siberia and China: proton microprobe studies. International symposium on Cenozoic volcanic rocks and deep-seated xenoliths of China and its Environs. Beijing, p. 20.

Griffin, W.L., et al., 2000. The Hf isotope composition of cratonic mantle: LAM-MC-ICPMS analysis of zircon megacrysts in kimberlites. Geochim. Cosmochim. Acta 64, 133–147.

Grunder, A.L., 1995. Material and thermal roles of basalt in crustal magmatism — case study from eastern Nevada. Geology 23, 952–956.

Guo, F., Fan, W.M., Wang, Y.J., Zhang, M., 2004. Origin of early Cretaceous calc-alkaline lamprophyres from the Sulu orogen in eastern China: implications for enrichment processes beneath continental collisional belt. Lithos 78, 291–305.

Gwalani, L.G., Rock, N.M.S., Ramasamy, R., Griffin, B.J., Mulai, B.P., 2000. Complexly zoned Ti-rich melanite–schorlomite garnets from Ambadungar carbonatite–alkalic complex, Deccan Igneous Province, Gujarat State, Western India. J. Asian Earth Sci. 18, 163–176.

Hart, S.R., 1984. A large-scale isotope anomaly in the southern hemisphere mantle. Nature 309, 753–757.

Huang, J., 1991. Petrology and petrogenesis of Zijinshan alkaline ring complex from Linxian County, Shanxi Province, China. Mod. Geosci. 5, 24–29 (in Chinese with English abstract).

Jahn, B.M., Zhang, Z.Q., 1984. Archean granulite gneisses from eastern Hebei Province, China: rare earth geochemistry and tectonic implications. Contrib. Mineral. Petrol. 85, 224–243.

Jahn, B.M., et al., 1987. 3.5 Ga old amphibolites from eastern Hebei Province, China — field occurrence, petrography, Sm–Nd isochron age and REE geochemistry. Precambrian Res. 34, 311–346.

Jahn, B.M., Wu, F.Y., Lo, C.H., Tsai, C.H., 1999. Crust-mantle interaction induced by deep subduction of the continental crust: geochemical and Sr–Nd isotopic evidence from post-collisional mafic–ultramafic intrusions of the northern Dabie complex, central China. Chem. Geol. 157, 119–146.

Please cite this article as: Ying, J. et al. Petrology and geochemistry of Zijinshan alkaline intrusive complex in Shanxi Province, western North China Craton: Implication for magma mixing of different sources in an extensional regime. Lithos (2007), doi:10.1016/j.lithos.2007.02.001

Kimura, G., Takahashi, M., Kono, M., 1990. Mesozoic collision-extrusion tectonics in eastern Asia. Tectonophysics 181, 15–23.

Leake, B.E., et al., 1997. Nomenclature of amphiboles; report of the subcommittee on amphiboles of the International Mineralogical Association, Commission on New Minerals and Mineral Names. Am. Mineral. 82, 1019–1037.

Litvinovsky, B.A., Jahn, B.M., Zanvilevich, A.N., Shadaev, M.G., 2002. Crystal fractionation in the petrogenesis of an alkali monzodiorite-syenite series: the Oshurkovo plutonic sheeted complex, Transbaikalia, Russia. Lithos 64, 97–130.

Liu, D.Y., Nutman, A.P., Compston, W., Wu, J.S., Shen, Q.H., 1992. Remnants of ≥3800 Ma crust in the Chinese part of the Sino–Korean Craton. Geology 20, 339–342.

Lubala, R.T., Frick, C., Rogers, J.H., Walraven, F., 1994. Petrogenesis of syenites and granites of the Schiel Alkaline Complex, Northern Transvaal, South Africa. J. Geol. 102, 307–316.

Lynch, D.J., Musselman, T.E., Gutmann, J.T., Patchett, P.J., 1993. Isotopic evidence for the origin of Cenozoic volcanic rocks in the Pinacate Volcanic Field, Northwestern Mexico. Lithos 29, 295–302.

Ma, X.Y., 1989. Atlas of Active Fault of China. Seismologic Press, Beijing. 120 pp.

Maruyama, S., Send, T., 1986. Orogeny and relative plate motions: example of the Japanese Islands. Tectonophysics 127, 305–329.

Meng, Q.R., 2003. What drove late Mesozoic extension of the northern China–Mongolia tract? Tectonophysics 369, 155–174.

Menzies, M.A., Fan, W.M., Zhang, M., 1993. Paleozoic and Cenozoic lithoprobes and the loss of >120 km of Archean lithosphere, Sino–Korean Craton, China. In: Prichard, H.M., Alabaster, T., Harris, N.B.W., Neary, C.R. (Eds.), Magmatic Processes and Plate Tectonics. Geological Society Special Publication, pp. 71–81.

Morimoto, N., 1988. Nomenclature of pyroxenes. Mineral. Mag. 52, 535–550.

Pervov, V.A., et al., 1997. Potassic magmatism of the Aldan Shield, Southeastern Siberia: an indicator of the multistage evolution of the lithospheric mantle. Petrology 5, 415–430.

Petford, N., Gallagher, K., 2001. Partial melting of mafic (amphibolitic) lower crust by periodic influx of basaltic magma. Earth Planet. Sci. Lett. 193, 483–499.

Pouchou, J.L., Pichoir, F., 1991. Quantitative analysis of homogeneous or stratified microvolumes applying the model "PAP". In: Heinrich, K.F.J., Newbury, D.E. (Eds.), Electron Probe Quantification. Plenum, New York, pp. 31–75.

Rapp, R.P., Watson, E.B., 1995. Dehydration melting of metabasalt at 8–32 kbar: implications for continental growth and crust–mantle recycling. J. Petrol. 36, 891–931.

Shao, J.A., Mu, B.L., Zhang, L., 2000. Deep geological process and its shallow response during Mesozoic transfer of tectonic framework in eastern North China. Geol. Rev. 46, 32–40 (in Chinese with English abstract).

Sheppard, S., 1995. Hybridization of shoshonitic lamprophyre and calc-alkaline granite magma in the early Proterozoic Mt Bundey igneous suite, Northern-Territory. Aust. J. Earth Sci. 42, 173–185.

Söderlund, U., Patchett, P.J., Vervoort, J.D., Isachsen, C.E., 2004. The ^{176}Lu decay constant determined by Lu–Hf and U–Pb isotope systematics of Precambrian mafic intrusions. Earth Planet. Sci. Lett. 219, 311–324.

Sun, S.S., McDonough, W.F., 1989. Chemical and isotopic systematics of oceanic basalts: implications for mantle composition and processes. In: Saunders, A.D., Norry, M.J. (Eds.), Magmatism in the Oceanic Basalts. Geological Society Special Publication, pp. 313–345.

Tang, Y.J., Zhang, H.F., Ying, J.F., 2006. Asthenosphere–lithospheric mantle interaction in an extensional regime: implication from the geochemistry of Cenozoic basalts from Taihang Mountains, North China Craton. Chem. Geol. 233, 309–327.

Wang, Y.J., Fan, W.M., Zhang, H.F., Peng, T.P., 2006. Early Cretaceous gabbroic rocks from the Taihang Mountains: implications for a paleosubduction-related lithospheric mantle beneath the central North China Craton. Lithos 86, 281–302.

Wolf, M.B., Wyllie, P.J., 1994. Dehydration-melting of amphibolite at 10 kbar: the effects of temperature and time. Contrib. Mineral. Petrol. 115, 369–383.

Wright, J.B., 1969. A simple alkalinity ratio and its application to questions of non-orogenic granite genesis. Geol. Mag. 106, 370–384.

Wu, L.R., Zhang, Z.Z., Zhang, Y.X., 1966. The petrogenesis and mineralization of alkaline rocks in Shanxi Province. In: Wu, L.R. (Ed.), The Studies of Alkaline Rocks from Several Regions in China. Science Press, Beijing, pp. 1–76.

Wu, F.Y., Yang, Y.H., Xie, L.W., Yang, J.H., Xu, P., 2006. Hf isotopic compositions of the standard zircons and baddeleyites used in U–Pb geochronology. Chem. Geol. 234, 105–126.

Xu, Y.G., 2001. Thermo-tectonic destruction of the Archaean lithospheric keel beneath the Sino–Korean Craton in China: evidence, timing and mechanism. Phys. Chem. Earth 26, 747–757.

Xu, Y.G., Chung, S.L., Ma, J.L., Shi, L.B., 2004. Contrasting Cenozoic lithospheric evolution and architecture in the western and eastern Sino–Korean Craton: constraints from geochemistry of basalts and mantle xenoliths. J. Geol. 112, 593–605.

Yan, G.H., Mou, B.L., Zeng, Y.S., 1988. The characteristics of REE, Sr and O isotops of the Zijinshan alkaline–carbonatites complex, Shanxi. Acta Petrol. Sin. 3, 29–35 (in Chinese).

Yan, G.H., et al., 2000. Geochronology and isotopic features of Sr, Nd, and Pb of the Triassic alkali intrusions in the Yanshan–Yinshan regions. Sci. China, Ser. D: Earth Sci. 30, 384–387.

Ying, J.F., Zhou, X.H., Zhang, H.F., 2004. Geochemical and isotopic investigation of the Laiwu–Zibo carbonatites from western Shandong Province, China, and implications for their petrogenesis and enriched mantle source. Lithos 75, 413–426.

Ying, J.F., Zhang, H.F., Kita, N., Morishita, Y., Shimoda, G., 2006. Nature and evolution of Late Cretaceous lithospheric mantle beneath the eastern North China Craton: Constraints from petrology and geochemistry of peridotitic xenoliths from Jünan, Shandong Province, China. Earth Planet. Sci. Lett. 244, 622–638.

Yuan, H.L., et al., 2004. Accurate U–Pb age and trace element determinations of zircons by laser ablation inductively coupled plasma mass spectrometry. Geostand. Newsl. 28, 353–370.

Zhang, H.F., 2005. Transformation of lithospheric mantle through peridotite-melt reaction: a case of Sino–Korean Craton. Earth Planet. Sci. Lett. 237, 768–780.

Zhang, H.F., Sun, M., 2002. Geochemistry of Mesozoic basalts and mafic dikes, southeastern North China Craton, and tectonic implications. Int. Geol. Rev. 44, 370–382.

Zhang, H.F., et al., 2002. Mesozoic lithosphere destruction beneath the North China Craton: evidence from major-, trace-element and Sr–Nd–Pb isotope studies of Fangcheng basalts. Contrib. Mineral. Petrol. 144, 241–254.

Zhang, H.F., et al., 2003. Secular evolution of the lithosphere beneath the eastern North China Craton: evidence from Mesozoic basalts and high-Mg andesites. Geochim. Cosmochim. Acta 67, 4373–4387.

Zhang, H.F., Sun, M., Zhou, M.F., Fan, W.M., 2004. Highly heterogeneous late Mesozoic lithospheric mantle beneath the North China Craton: evidence from Sr–Nd–Pb isotopic systematic of mafic igneous rocks. Geol. Mag. 141, 55–62.

Please cite this article as: Ying, J. et al. Petrology and geochemistry of Zijinshan alkaline intrusive complex in Shanxi Province, western North China Craton: Implication for magma mixing of different sources in an extensional regime. Lithos (2007), doi:10.1016/j.lithos.2007.02.001

ARTICLE IN PRESS

Zhang, H.F., Sun, M., Zhou, X.H., Ying, J.F., 2005. Geochemical constraints on the origin of Mesozoic alkaline intrusive complexes from the North China Craton and tectonic implications. Lithos 81, 297–317.

Zhao, J.X., Shiraishi, K., Ellis, D.J., Sheraton, J.W., 1995. Geochemical and isotopic studies of syenites from the Yamato Mountains, East Antarctica — implications for the origin of syenitic magmas. Geochim. Cosmochim. Acta 59, 1363–1382.

Zhao, G.C., Wilde, S.A., Cawood, P.A., Sun, M., 2001. Archean blocks and their boundaries in the North China Craton: lithological, geochemical, structural and P–T path constraints and tectonic evolution. Precambrian Res. 107, 45–73.

Zhao, G.C., Wilde, S.A., Cawood, P.A., Sun, M., 2002. SHRIMP U–Pb zircon ages of the Fuping Complex: implications for late Archean to Paleoproterozoic accretion and assembly of the North China Craton. Am. J. Sci. 302, 191–226.

Zheng, Y.D., et al., 1996. Great Jurassic thrust sheets in Beishan (North Mountains)–Gobi area of China and southern Mongolia. J. Struct. Geol. 18, 1111–1126.

Zhou, L.D., Zhao, Z.H., Zhou, G.F., 1996. Isotopic chronology and some alkaline rock bodies in China. Geochimica 25, 164–171 (in Chinese with English abstract).

Zhou, X.H., Sun, M., Zhang, G.H., Chen, S.H., 2002. Continental crust and lithospheric mantle interaction beneath North China: isotopic evidence from granulite xenolith in Hannuoba, Sino–Korean Craton. Lithos 62, 111–124.

Zindler, A., Hart, S.R., 1986. Chemical geodynamics. Annu. Rev. Earth Planet. Sci. 14, 493–571.

Zou, H.B., Zindler, A., Xu, X.S., Qi, Q., 2000. Major, trace element, and Nd, Sr and Pb isotope studies of Cenozoic basalts in SE China: mantle sources, regional variations, and tectonic significance. Chem. Geol. 171, 33–47.

Zou, H.B., et al., 2003. Constraints on the origin of historic potassic basalts from northeast China by U–Th disequilibrium data. Chem. Geol. 200, 189–201.

Please cite this article as: Ying, J. et al. Petrology and geochemistry of Zijinshan alkaline intrusive complex in Shanxi Province, western North China Craton: Implication for magma mixing of different sources in an extensional regime. Lithos (2007), doi:10.1016/j.lithos.2007.02.001